# Supporting Information for

# Hypervalent Organoiodine(V) Metal-Organic Frameworks: Syntheses, Thermal Studies and Stoichiometric Oxidants

*Macguire Bryant[†] and Christopher Richardson[†]*

[†]School of Chemistry and Molecular Bioscience, University of Wollongong, Northfields Avenue, Wollongong, NSW 2522, Australia

## Contents

1. Synthesis Procedures ..... 2
   1.1. Synthesis of $Me_2$bpdc-I ..... 2
   1.2. Synthesis of $H_2$bpdc-I ..... 3
   1.3. Synthesis of $Me_2$bpdc-IO ..... 5
   1.4. Synthesis of $H_2$bpdc-IO ..... 5
   1.5. Preliminary Oxidation Experiments and Control Experiments for Benzyl Alcohol and Thioanisole ..... 5
2. SCXRD Analysis of $Me_2$bpdc-I and $H_2$bpdc-I ..... 6
3. Infrared Spectroscopic Data ..... 9
4. PXRD Data ..... 11
5. Differential Scanning Calorimetry-Thermogravimetric Analyses ..... 14
6. $^1$H NMR Spectroscopic Data ..... 19
7. Mass Spectrometric Data ..... 22
8. XPS Data ..... 23
   8.1. XPS spectra of $H_2$bpdc-I ..... 23
   8.2. XPS spectra of $H_2$bpdc-IO ..... 24
   8.3. XPS spectra of Iodoxybenzene, Ph-$IO_2$ ..... 26
   8.4. XPS spectra of $Zn_4O$(bpdc-I)$_3$ ..... 27
   8.5. XPS spectra of $Zn_4O$(bpdc-$IO_x$)$_3$ ..... 29
   8.6. XPS spectra of $Zr_6O_4(OH)_4$(bpdc-I)$_6$ ..... 30
   8.7. XPS spectra of $Zr_6O_4(OH)_4$(bpdc-$IO_x$)$_6$ ..... 32
   8.8. XPS spectra of $Zr_6O_4(OH)_4$(bpdc-$IO_x$)$_6$ Post-Thermolysis ..... 33
9. $N_2$ Gas Sorption at 77 K ..... 35
10. Gas Chromatography – Mass Spectrometry ..... 39
11. References ..... 40

# 1. Synthesis Procedures

DMDO was synthesised according to the procedure of Taber *et al.*[1]

## 1.1. Synthesis of $Me_2$bpdc-I

$NaNO_2$ (115.6 mg, 1.68 mmol) dissolved in distilled $H_2O$ (1 $cm^3$) and cooled to ice bath temperature was added dropwise over 30 minutes with stirring to dimethyl 2-amino-[1,1'-biphenyl]-4,4'-dicarboxylate (398.4 mg, 1.40 mmol) dissolved in 1:1 distilled $H_2O$:16M HCl solution (7.5 $cm^3$) at ice-bath temperature. The resulting mixture was left to stir for one hour at ice-salt bath temperature, before KI (398.4 mg, 2.40 mmol) was added with stirring. The solution was brought to room temperature and stirred for one hour, before being heated to 65 °C for three hours. The cooled solution was diluted with $H_2O$, before EtOAc was added. The $H_2O$ and EtOAc solutions were agitated together, with sodium sulfite added until the organic solution became pale yellow. The organic solution was removed, placed into a separatory funnel, and washed three times with $H_2O$, once with brine, dried over $Na_2SO_4$ and rotary evaporated under reduced pressure to give a white powder. The powder was recrystallised from hexane/$CH_2Cl_2$ to produce colourless crystals ($R_f$ = 0.38, 4:1 $CH_2Cl_2$:Hexane). Yield = 459.3 mg (83%). $^1$H NMR $\delta_H$ (400 MHz; $CDCl_3$) 3.96 (6 H, s); 7.36 (1 H, d, *J* = 7.92 Hz); 7.43 (2 H, m); 8.07 (1 H, dd, *J* = 1.60, 7.88 Hz); 8.13 (2 H, m); 8.63 (1 H, d, *J* = 1.60 Hz). $^{13}$C NMR $\delta_C$ (101 MHz; $CDCl_3$) 52.92, 53.15, 98.04, 129.80, 129.95, 130.13, 130.35, 130.54, 131.60, 141.40, 148.28, 150.59, 165.96, 167.38.

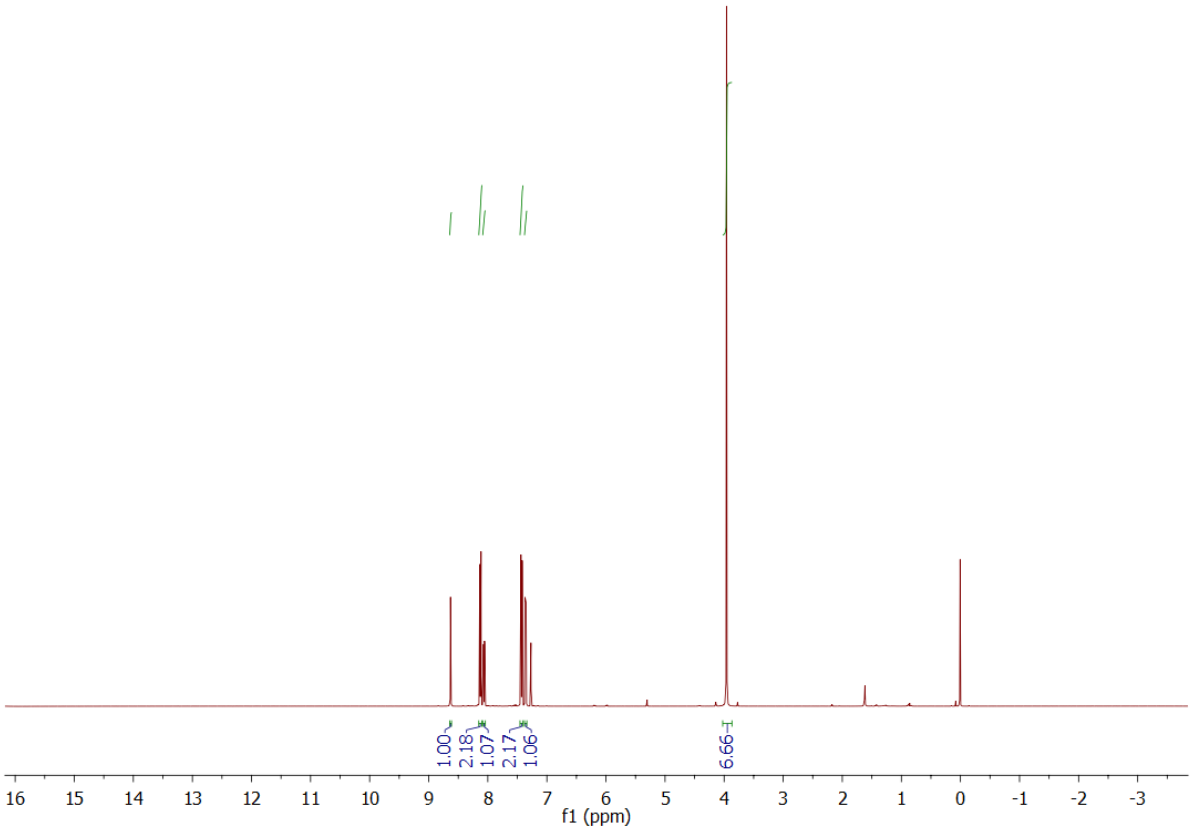

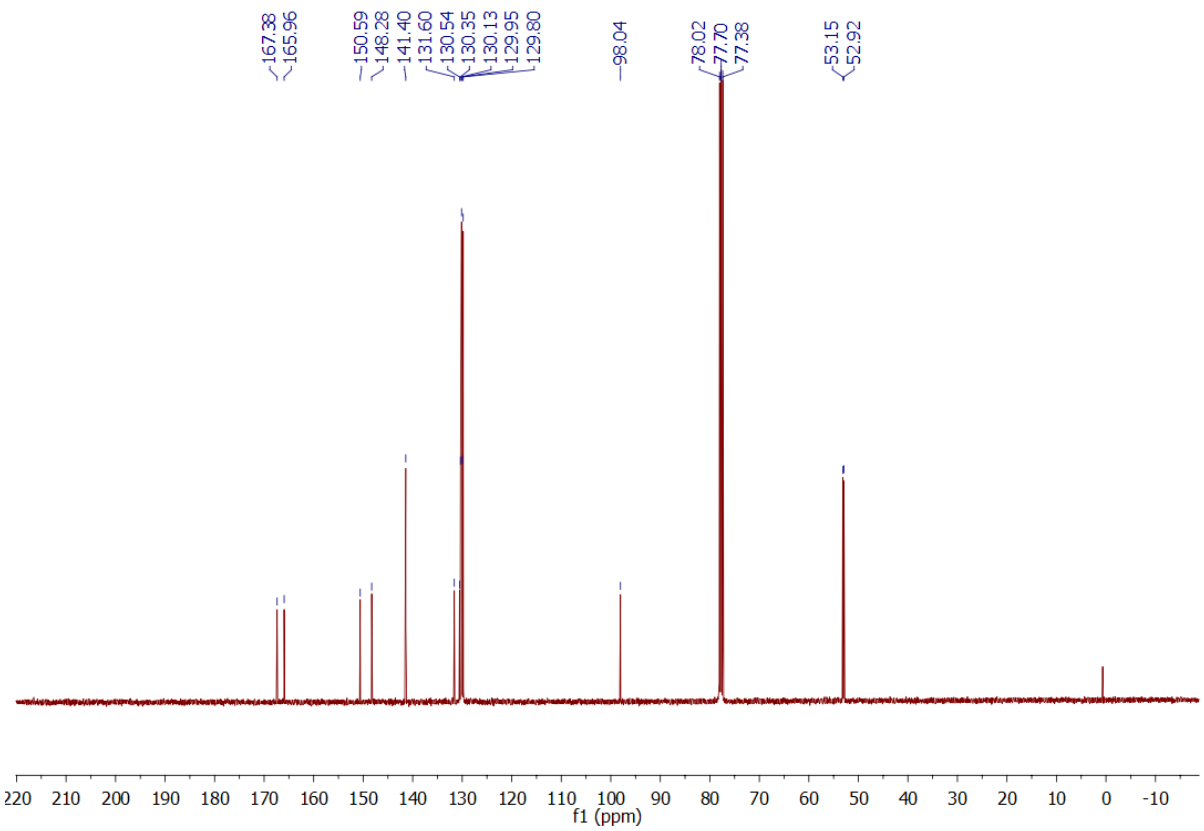


## 1.2. Synthesis of $H_2$bpdc-I

1.0 M NaOH solution (2.10 $cm^3$, 2.10 mmol) was added dropwise with stirring to dimethyl 2-iodo-[1,1'-biphenyl]-4,4'-dicarboxylate (332.6 mg, 0.840 mmol) dissolved in MeOH (20 $cm^3$) and THF (5 $cm^3$). The solution was stirred overnight at room temperature, before MeOH and THF were rotary evaporation under reduced pressure. The aqueous solution was diluted with water then acidified with 1.0 M HCl with stirring until no more precipitation was observed. The white solid was filtered and washed with three portions of $H_2O$. The off-white powder was dried in the fume hood for 18 hours. Yield = 287.6 mg (93%). ESI-MS Found: $[M-H]^-$ = 367 *m/z*. Calc. $H_2$bpdc-I ($C_{14}H_9IO_4$); C: 45.68%; H: 2.46%; Found C: 45.92%; H: 2.53%. $^1$H NMR $\delta_H$ (300 MHz; $d_6$-DMSO) 7.48 (3 H, m); 8.02 (3 H, m); 8.47 (1 H, d, *J* = 1.64 Hz). $^{13}$C NMR $\delta_C$ (100 MHz; $d_6$-DMSO) 98.19, 129.24, 129.28, 130.17, 130.47, 131.82, 139.96, 147.05, 149.20, 165.70, 167.04.

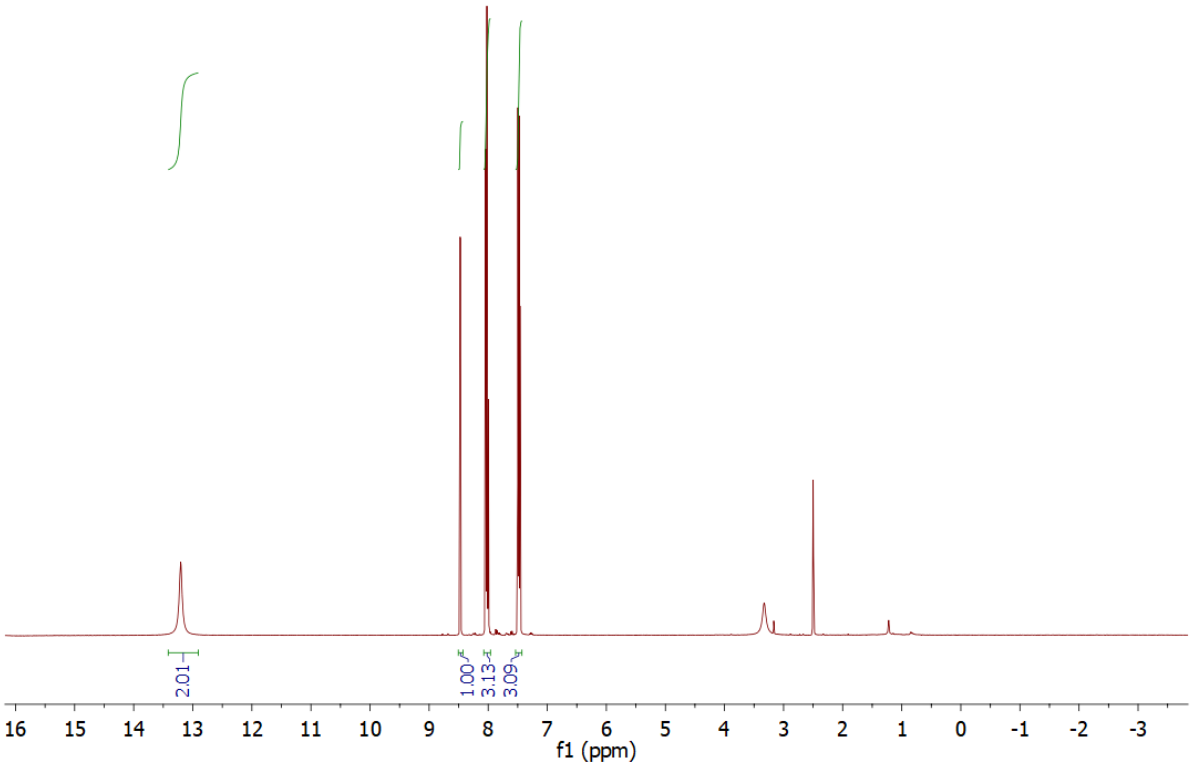
2.01
1.00
3.13
3.09
16 15 14 13 12 11 10 9 8 7 6 5 4 3 2 1 0 -1 -2 -3
f1 (ppm)

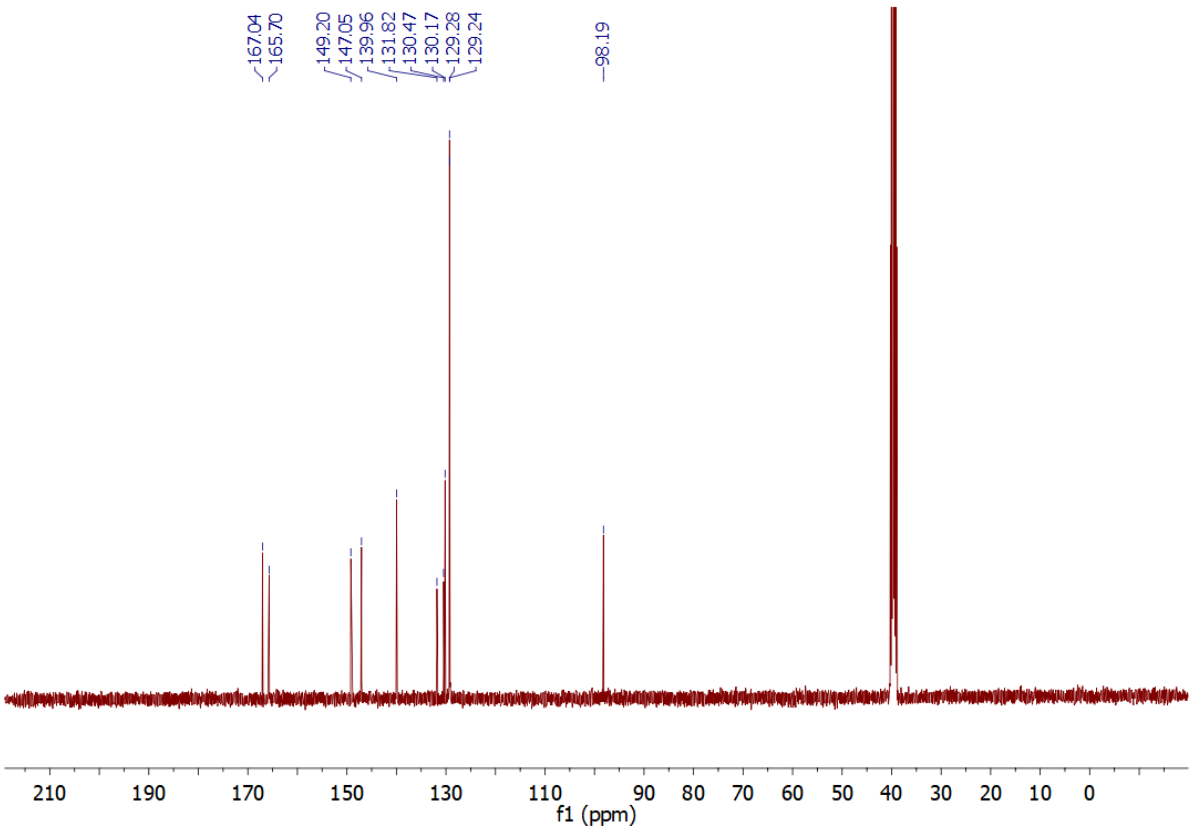
167.04
165.70
149.20
147.05
139.96
131.82
130.47
130.17
129.28
129.24
98.19
210 190 170 150 130 110 90 80 70 60 50 40 30 20 10 0
f1 (ppm)

## 1.3. Synthesis of $Me_2$bpdc-IO

A portion of 80 mM solution of DMDO in acetone (3.5 $cm^3$, 0.28 mmol) was added to $Me_2$bpdc-I (20 mg, 0.050 mmol) dissolved in acetone (0.5 $cm^3$). The vial was then capped and placed in a 4 °C fridge overnight. The crystalline material that formed was collected by filtration and washed with acetone. Yield = 10.9 mg (53%); Calc. $Me_2$bpdc-IO·$H_2O$ ($C_{16}H_{15}IO_6$); C: 44.86%; H: 3.06%; Found C: 44.66%; H: 2.48%.

## 1.4. Synthesis of $H_2$bpdc-IO

A portion of 80 mM DMDO in acetone solution (3.5 $cm^3$, 0.28 mmol) was added to $H_2$bpdc-I (20 mg, 0.054 mmol) dissolved in THF (0.5 $cm^3$). The vial was then capped and placed in a 4°C fridge overnight, before the cap was removed and the suspension being left to dry in a fume cupboard to produce a white precipitate. Yield = 13.8 mg (67%); Calc. $H_2$bpdc-IO·THF ($C_{18}H_{17}IO_6$) C: 47.37%; H: 3.67%; Found C: 47.39%; H: 3.11%.

To produce crystalline samples, a portion of 105 mM solution of DMDO in acetone (3 $cm^3$, 0.32 mmol) was added to $H_2$bpdc-I (10 mg, 0.027 mmol) dissolved in DMSO (1 $cm^3$). The vial was then capped and placed in a 4 °C fridge overnight. Slow evaporation of the solution over three weeks produced small colourless crystals, which were collected by filtration and washed with acetone.

## 1.5. Preliminary Oxidation Experiments and Control Experiments for Benzyl Alcohol and Thioanisole

We carried out some preliminary experiments to establish if an activating acid was required in the oxidation reactions using $Zr_6O_4(OH)_4$(bpdc-I$O_x$)$_6$ and performed some control reactions with $Zr_6O_4(OH)_4$(bpdc-I)$_6$ *i.e.* the MOF in the unreactive I(I) state. Our method was to dry portions of $Zr_6O_4(OH)_4$(bpdc-I)$_6$ or $Zr_6O_4(OH)_4$(bpdc-I$O_x$)$_6$ (100 °C for 1 hour and cooled under vacuum) in pre-weighed dry vials and use the mass of activated MOF (typically ~30 mg) to calculate ~0.25 equivalents of substrate (benzyl alcohol or thioanisole) and trifluoroacetic acid. The substrates were added in $CDCl_3$ (1 $cm^3$) with and without the trifluoroacetic acid and the suspension was capped and stirred magnetically for 30 minutes then heated to 65 °C with stirring. Aliquots were taken and analysed by $^1$H NMR spectroscopy at various time points and returned to the reaction.

What we found was that:

1. No reactions proceeded with $Zr_6O_4(OH)_4$(bpdc-I)$_6$ either with or without trifluoroacetic acid and for each substrate over 72 hours.
2. Reactions proceeded only very slowly with $Zr_6O_4(OH)_4$(bpdc-I$O_x$)$_6$ often taking days to reach high levels of conversion.
3. Reactions proceeded to completion much more rapidly over a few hours for both substrates when trifluoroacetic acid was present in the same molar quantity as the substrate in reactions involving $Zr_6O_4(OH)_4$(bpdc-I$O_x$)$_6$.

## 2. SCXRD Analysis of $Me_2$bpdc-I and $H_2$bpdc-I

**Table S2.1:** Crystallographic data for $Me_2$bpdc-I

| | |
|---|---|
| **Identification code** | $Me_2$bpdc-I |
| **Empirical formula** | $C_{16}H_{13}IO_4$ |
| **Formula weight** | 396.16 |
| **Temperature/K** | 149.99(10) |
| **Crystal system** | triclinic |
| **Space group** | P-1 |
| **a/Å** | 7.8767(4) |
| **b/Å** | 10.0877(5) |
| **c/Å** | 10.6978(5) |
| **α/°** | 105.230(4) |
| **β/°** | 107.161(4) |
| **γ/°** | 102.068(4) |
| **Volume/Å³** | 744.83(7) |
| **Z** | 2 |
| **$\rho_{calc}$g/cm³** | 1.766 |
| **μ/mm⁻¹** | 2.162 |
| **F(000)** | 388.0 |
| **Crystal size/mm³** | 0.4 × 0.26 × 0.07 |
| **Radiation** | Mo Kα (λ = 0.71073) |
| **2Θ range for data collection/°** | 4.25 to 61.32 |
| **Index ranges** | -11 ≤ h ≤ 11, -14 ≤ k ≤ 14, -15 ≤ l ≤ 15 |
| **Reflections collected** | 14566 |
| **Independent reflections** | 4355 [$R_{int}$ = 0.0312, $R_{sigma}$ = 0.0231] |
| **Data/restraints/parameters** | 4355/0/192 |
| **Goodness-of-fit on F²** | 1.043 |
| **Final R indexes [I>=2σ(I)]** | $R_1$ = 0.0197, $wR_2$ = 0.0527 |
| **Final R indexes [all data]** | $R_1$ = 0.0217, $wR_2$ = 0.0533 |
| **Largest diff. peak/hole / e Å⁻³** | 0.97/-0.67 |

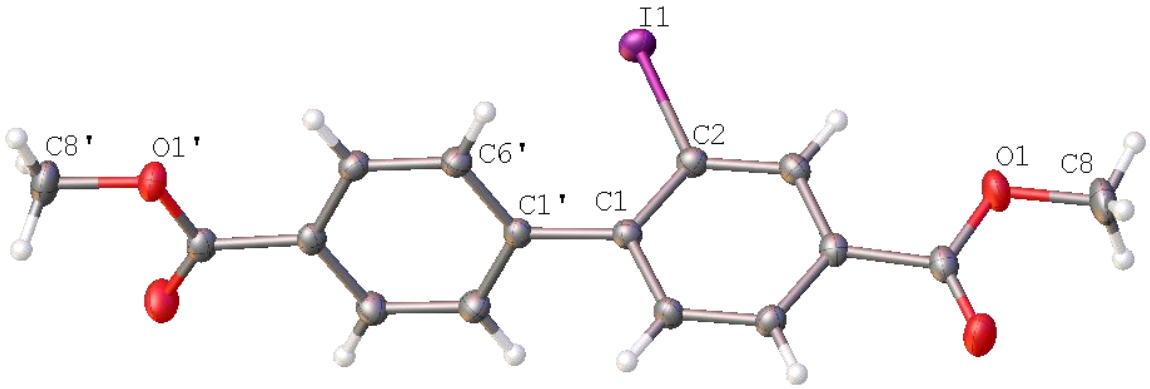


**Figure S2.1:** A perspective view of the asymmetric unit of $Me_2$bpdc-I with thermal ellipsoids at the 50% level. Selected distances and angles: C2-I1: 2.1036(18) Å, O1-C8 = O1'-O8': 1.445(3) Å, C2-C1-C1-C6: 71.4(3)°.

$Me_2$bpdc-I crystallises in the space group P-1 with one full molecule in the asymmetric unit. All hydrogen atoms were placed geometrically and refined in riding models on their carrier carbon atoms.

**Table S2.2:** Crystallographic data for $H_2$bpdc-I

| | |
|---|---|
| **Identification code** | $H_2$bpdc-I·DMSO |
| **Empirical formula** | $C_{16}H_{15}IO_5S$ |
| **Formula weight** | 446.24 |
| **Temperature/K** | 150.00(10) |
| **Crystal system** | triclinic |
| **Space group** | P-1 |
| **a/Å** | 8.19869(18) |
| **b/Å** | 8.27594(19) |
| **c/Å** | 13.9191(2) |
| **α/°** | 86.9929(16) |
| **β/°** | 74.1903(17) |
| **γ/°** | 69.153(2) |
| **Volume/Å$^3$** | 848.18(3) |
| **Z** | 2 |
| **$\rho_{calc}$g/cm$^3$** | 1.747 |
| **μ/mm$^{-1}$** | 2.032 |
| **F(000)** | 440.0 |
| **Crystal size/mm$^3$** | 0.38 × 0.32 × 0.09 |
| **Radiation** | Mo Kα (λ = 0.71073) |
| **2Θ range for data collection/°** | 5.274 to 61.406 |
| **Index ranges** | -11 ≤ h ≤ 11, -11 ≤ k ≤ 11, -19 ≤ l ≤ 18 |
| **Reflections collected** | 16754 |
| **Independent reflections** | 4989 [$R_{int}$ = 0.0184, $R_{sigma}$ = 0.0202] |
| **Data/restraints/parameters** | 4989/36/248 |
| **Goodness-of-fit on F$^2$** | 1.039 |
| **Final R indexes [I>=2σ (I)]** | $R_1$ = 0.0262, $wR_2$ = 0.0640 |
| **Final R indexes [all data]** | $R_1$ = 0.0342, $wR_2$ = 0.0676 |
| **Largest diff. peak/hole / e Å$^{-3}$** | 0.59/-1.39 |

$H_2$bpdc-I crystallises from DMSO solution as a disordered hydrogen-bonded solvate. The two positions of the DMSO were modelled together with the positions of the hydrogen of the carboxylic acid [0.544(3) : 0.456(3)]. The DMSO molecules were refined as rigid groups. All hydrogens were placed geometrically and allowed to ride on their carrier atoms. The hydrogen bond distances and angles are given in Table S2.3 below.

**Table S2.3:** Hydrogen Bonds for $H_2$bpdc-I·DMSO.

| D | H | A | d(D-H)/Å | d(H-A)/Å | d(D-A)/Å | D-H-A/° |
|---|---|---|---|---|---|---|
| **O4** | H4 | O3[1] | 0.82 | 1.81 | 2.6258(18) | 176.7 |

*[1]1-X,1-Y,2-Z*

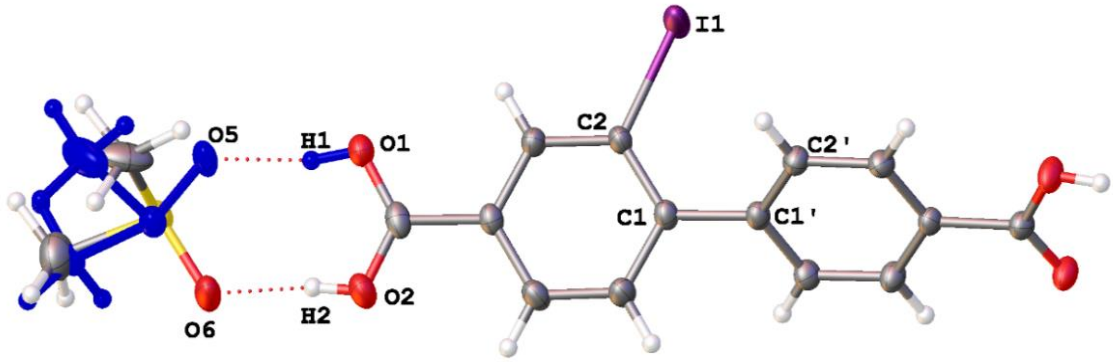


**Figure S2.2:** A perspective view, with ellipsoids at the 50% level, of the asymmetric unit of $H_2$bpdc-I showing the nature of the hydrogen bonding between the carboxylic acid and the disordered DMSO molecule. The minor disordered component is coloured blue for clarity. Selected distances and angles: C2-I1: 2.1035(17) Å; H1-O5: 1.716 Å; H2-O6: 1.693 Å; C2-C1-C1'-C2': 55.55(19)°.

## 3. Infrared Spectroscopic Data

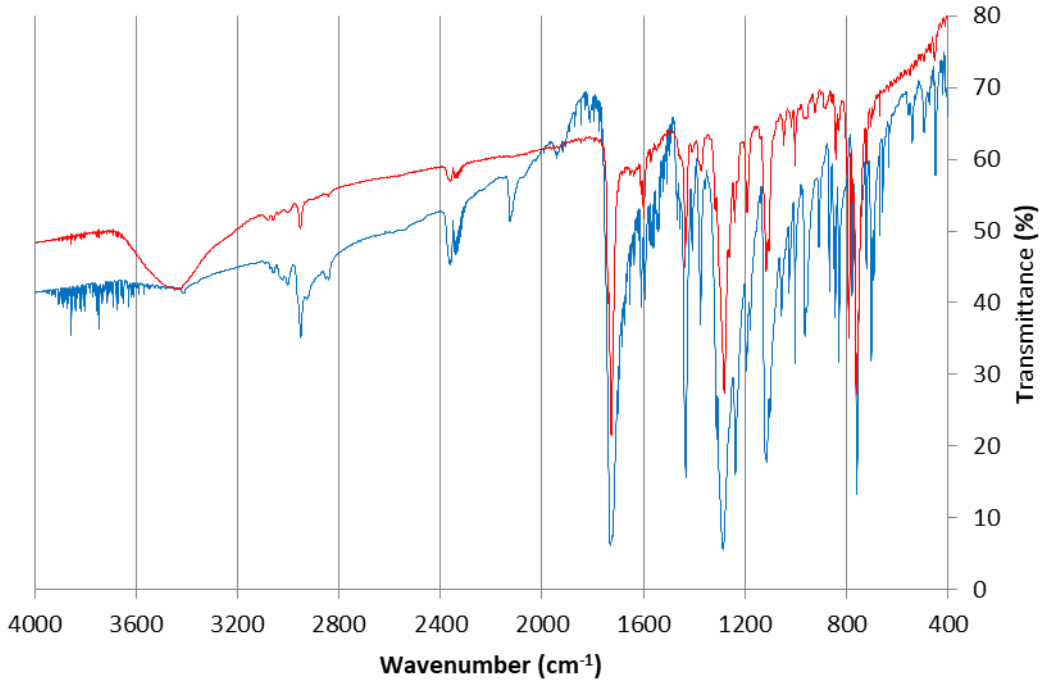


**Figure S3.1**: Infrared spectra of $Me_2$bpdc-I (blue) and $Me_2$bpdc-$IO_x$ (red) in KBr disks.

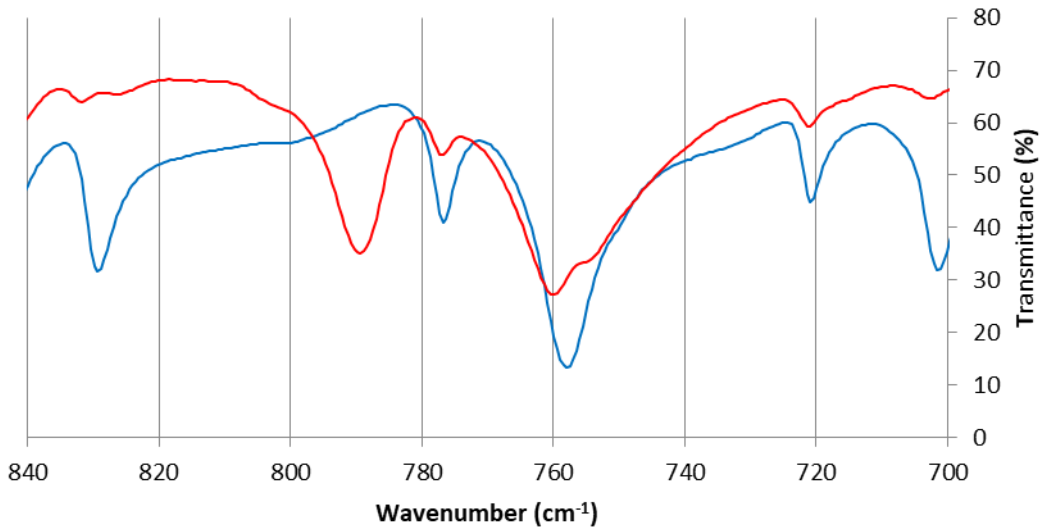


**Figure S3.2:** Detail infrared spectra of $Me_2$bpdc-I (blue) and $Me_2$bpdc-$IO_x$ (red) between 840 $cm^{-1}$ and 700 $cm^{-1}$. The I=O stretch is assigned as the band at 790 $cm^{-1}$.[2]

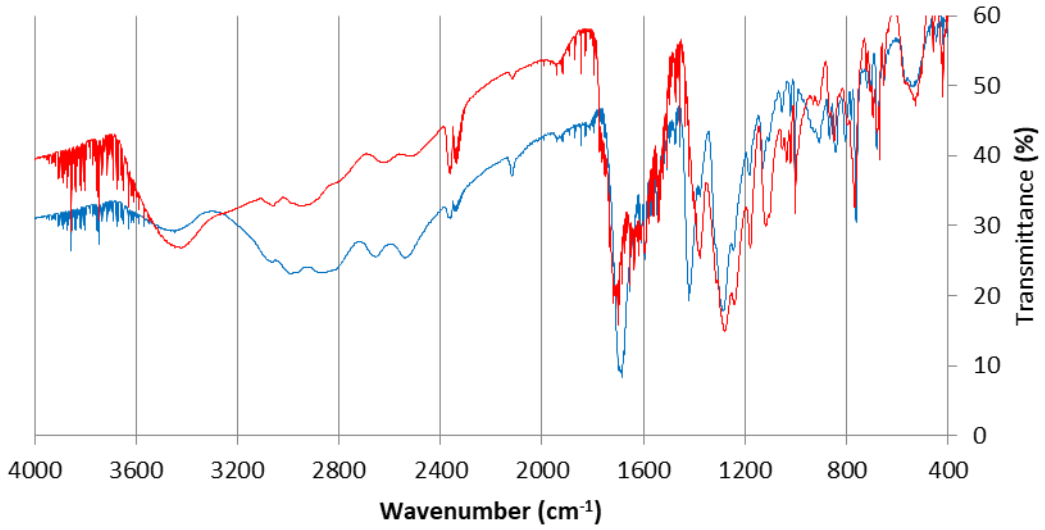


**Figure S3.3:** Infrared spectra of $H_2$bpdc-I (blue) and $H_2$bpdc-IO (red) in KBr disks.

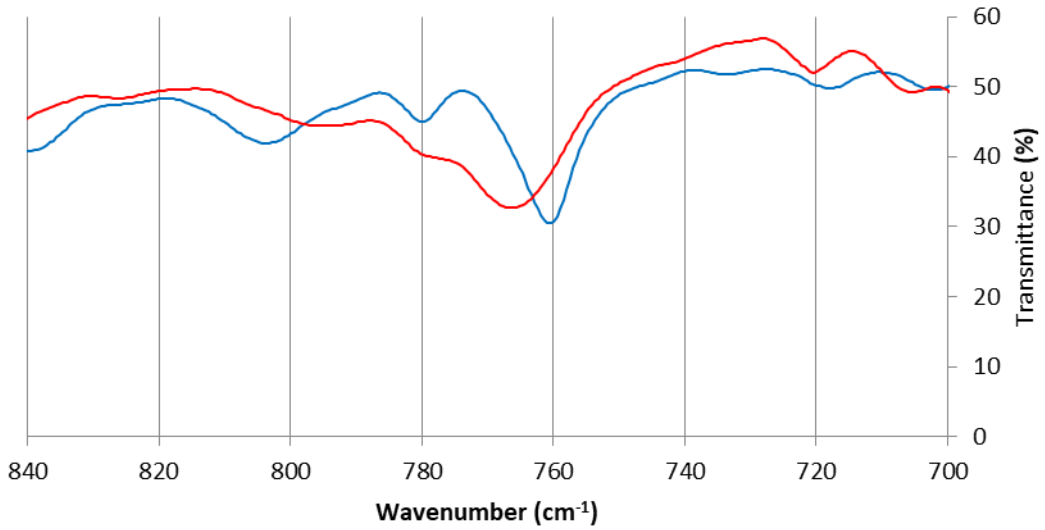


**Figure S3.4:** Detail infrared spectra of $H_2$bpdc-I (blue) and $H_2$bpdc-IO (red) between 840 $cm^{-1}$ and 700 $cm^{-1}$. I=O stretch is typically between 740-780 $cm^{-1}$.[2]

## 4. PXRD Data

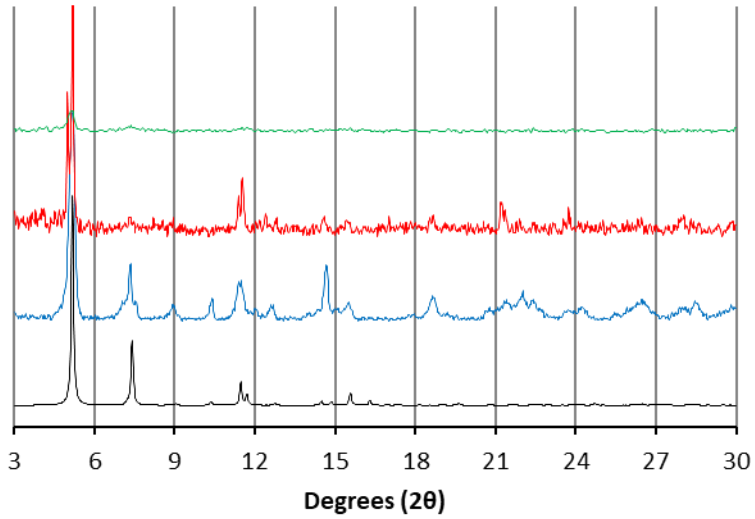


**Figure S4.1:** Calculated PXRD pattern of $Zn_4O(bpdc\text{-}I_2)_3$ (black),[3] and experimental PXRD patterns of $Zn_4O(bpdc\text{-}I)_3$ from acetone (blue), $Zn_4O(bpdc\text{-}IO_x)_3$ after activation (red, intensity multiplied by 3), and $Zn_4O(bpdc\text{-}IO_x)_3$ after thermolysis (green).

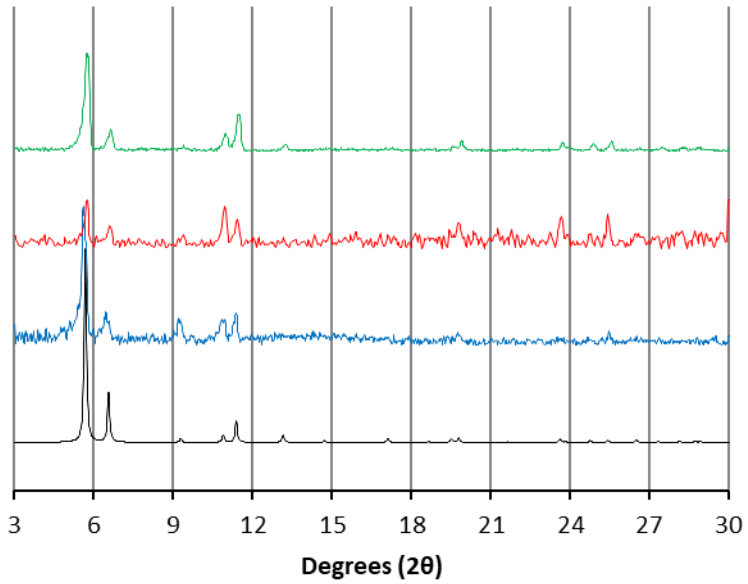


**Figure S4.2:** Calculated PXRD pattern of UiO-67 (black),[4] and PXRD patterns of as synthesised $Zr_6O_4(OH)_4(bpdc\text{-}I)_6$ (blue), $Zr_6O_4(OH)_4(bpdc\text{-}IO_x)_6$ under DMF (red), and $Zr_6O_4(OH)_4(bpdc\text{-}IO_x)_6$ after thermolysis (green).

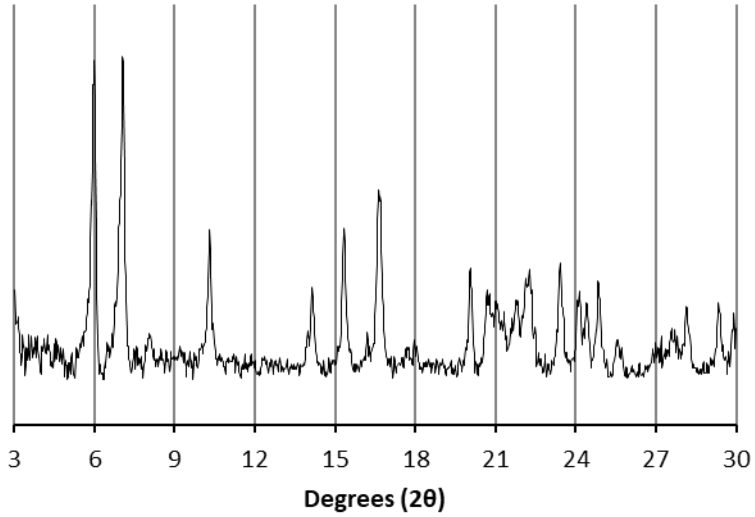


**Figure S4.3:** PXRD pattern of $Me_2$bpdc-IO.

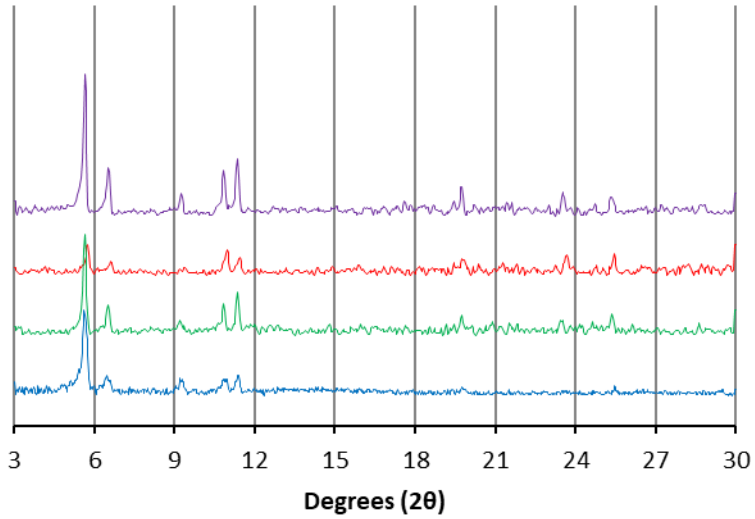


**Figure S4.4:** PXRD patterns of MOF samples before and after reaction with thioanisole and trifluoroacetic acid in $CDCl_3$; $Zr_6O_4(OH)_4$(bpdc-I)$_6$ before (blue) and after (green); $Zr_6O_4(OH)_4$(bpdc-$IO_x$)$_6$ before (red) and after (purple).

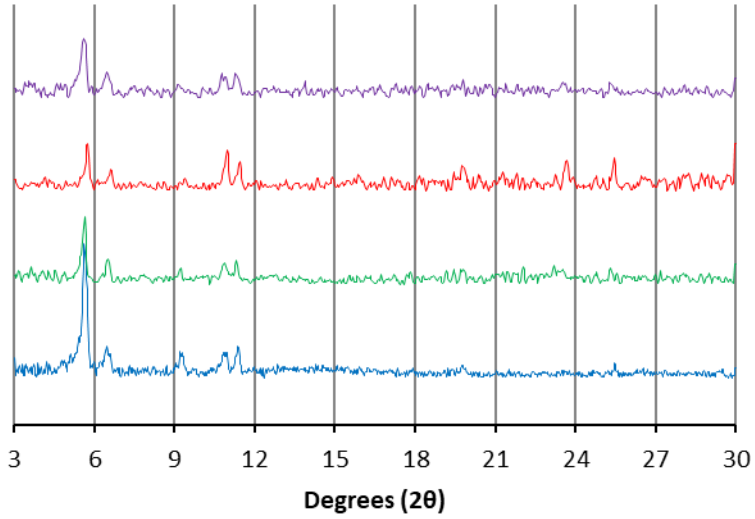


**Figure S4.5:** PXRD patterns of MOF samples before and after reaction with benzyl alcohol and trifluoroacetic acid in $CDCl_3$; $Zr_6O_4(OH)_4$(bpdc-I)$_6$ before (blue) and after (green); $Zr_6O_4(OH)_4$(bpdc-$IO_x$)$_6$ before (red) and after (purple).

## 5. Differential Scanning Calorimetry-Thermogravimetric Analyses

Safety note: Care must be taken when dealing with hypervalent iodine compounds as they are potentially explosive. We carried out thermal studies on small amounts of compounds and in the controlled environment of the DSC-TGA furnace.

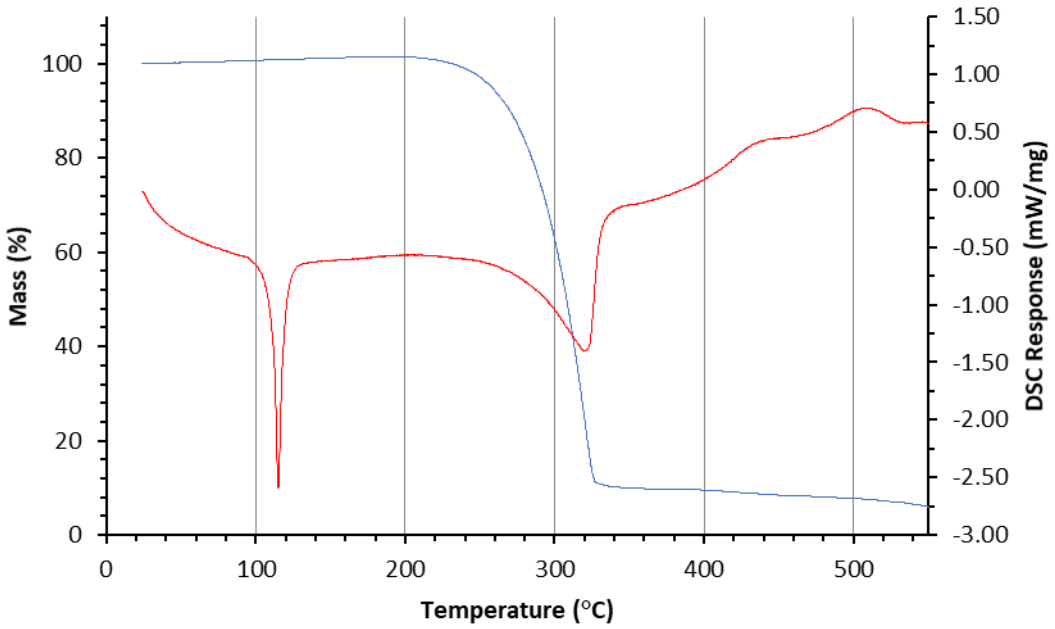


**Figure S5.1:** TG (blue line) and DSC (red line) traces of $Me_2$bpdc-I under a flow of $N_2$ (20 $cm^3$/min).

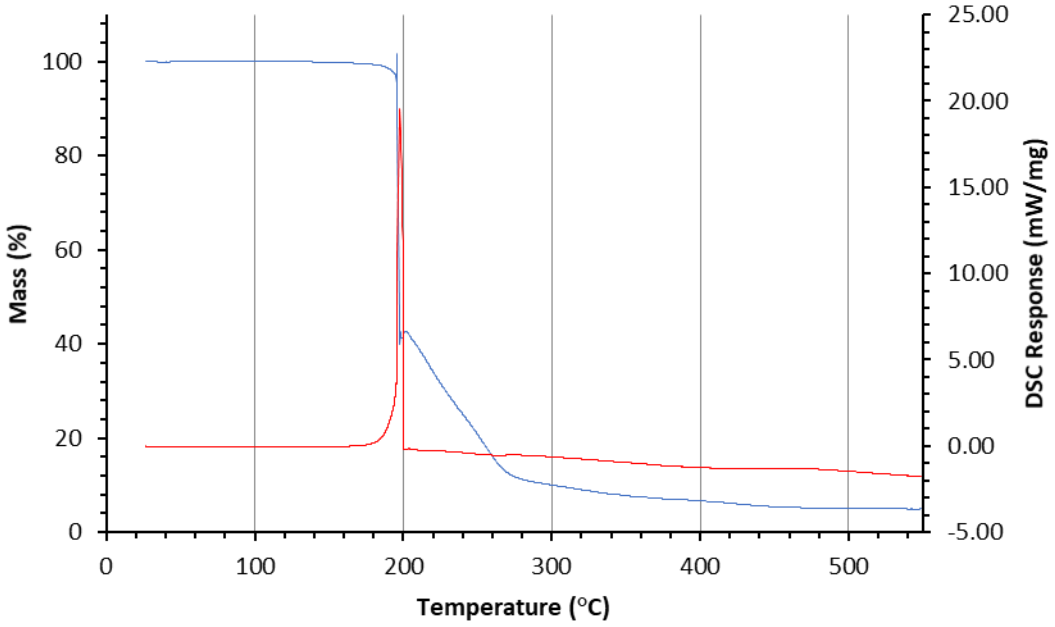


**Figure S5.2:** TG (blue line) and DSC (red line) traces of $Me_2$bpdc-IO under a flow of $N_2$ (20 $cm^3$/min). DSC response peaks at 19.60 mW/mg.

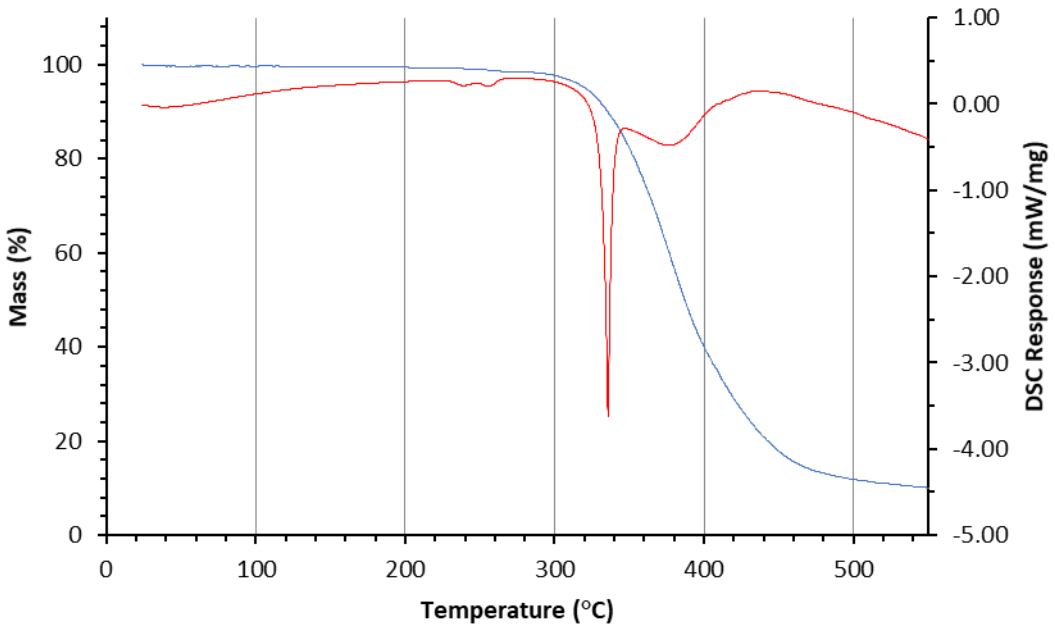


**Figure S5.3:** TG (blue line) and DSC (red line) traces of $H_2$bpdc-I under a flow of $N_2$ (20 $cm^3$/min).

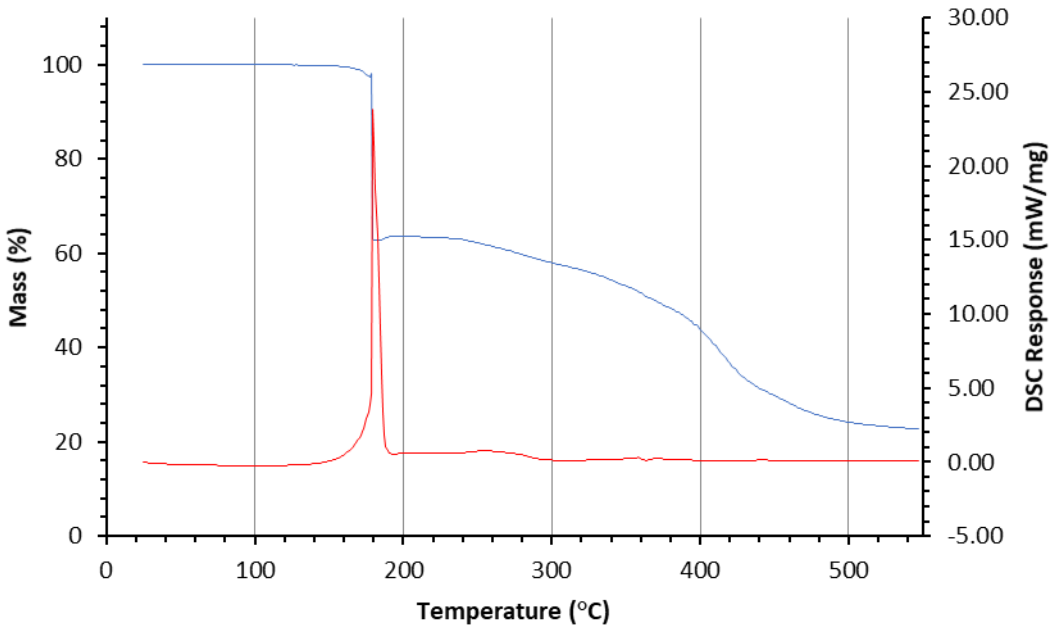


**Figure S 5.4:** TG (blue line) and DSC (red line) traces of $H_2$bpdc-IO crystallized from DMSO under a flow of $N_2$ (20 $cm^3$/min). DSC response peaks at 23.80 mW/mg.

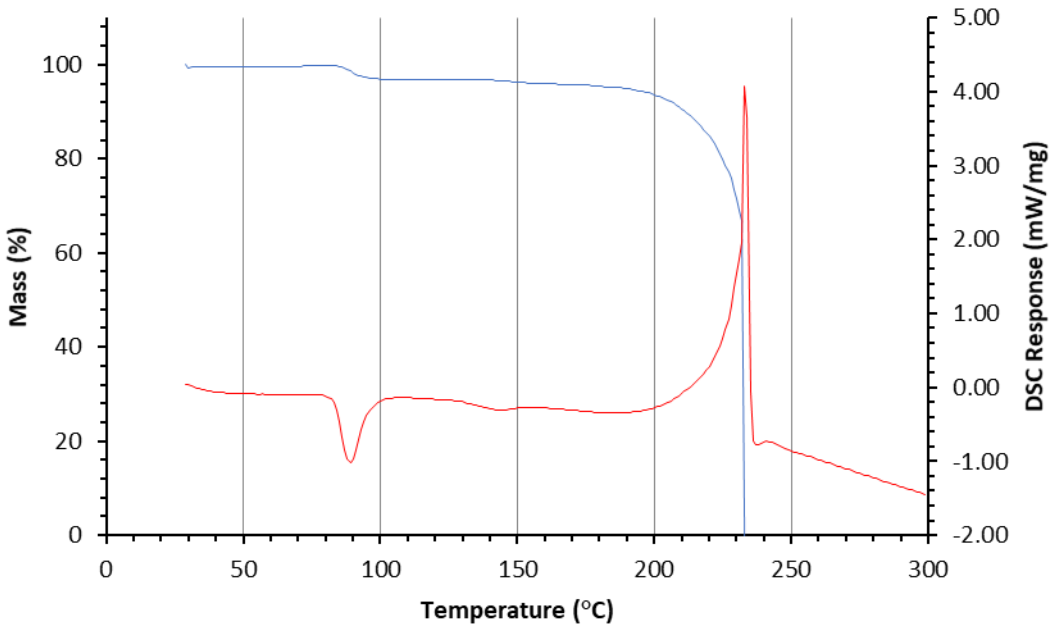


**Figure S5.5:** TG (blue line) and DSC (red line) traces of $PhIO_2$. Sample detonated at 233.4 °C. Performed on 3.1997 mg of material, heating at 5 °C/min to 300 °C under a flow of $N_2$ (40 $cm^3$/min). Decomposition is consistent with literature value of 230 °C.[5]

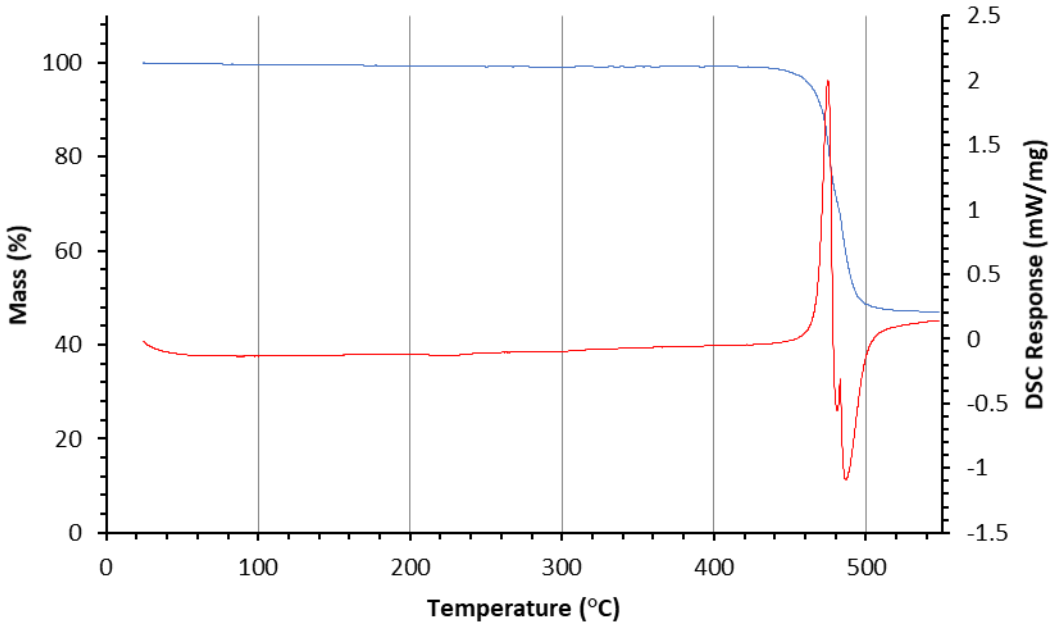


**Figure S5.6:** TG (blue line) and DSC (red line) traces of activated $Zn_4O(bpdc\text{-}I)_3$ under a flow of $N_2$ (20 $cm^3$/min).

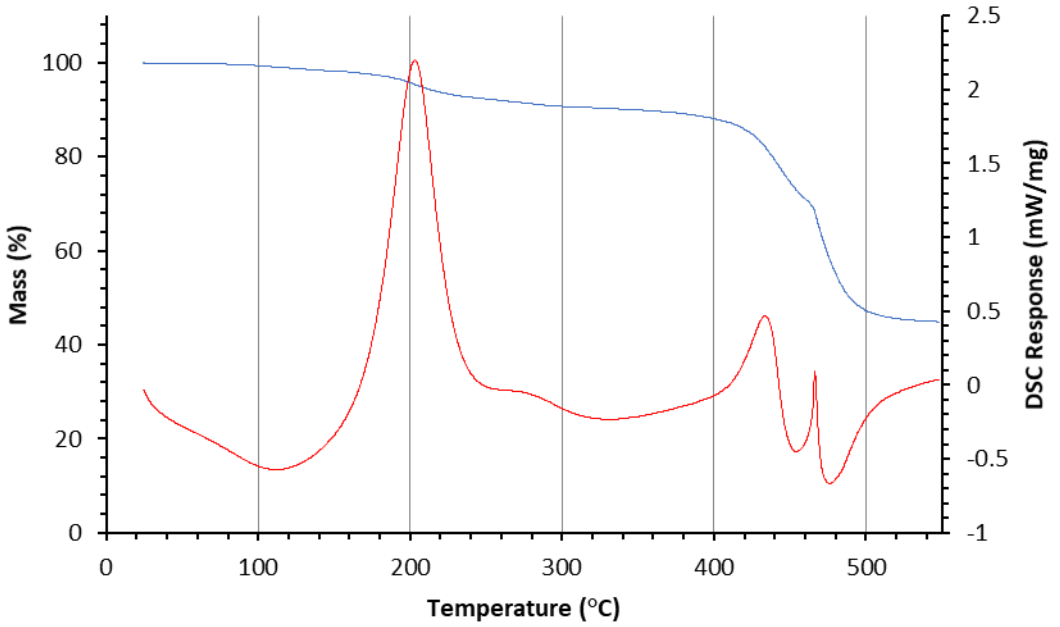


**Figure S5.7:** TG (blue line) and DSC (red line) traces of activated $Zn_4O(bpdc\text{-}IO_x)_3$ under a flow of $N_2$ (20 $cm^3$/min).

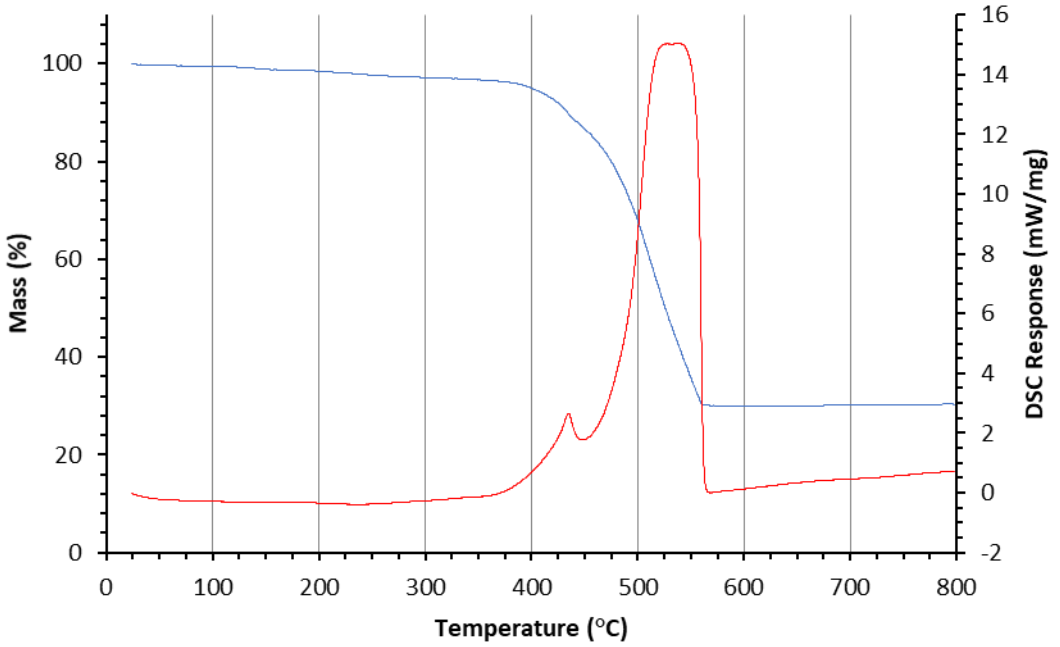


**Figure S5.8:** TG (blue line) and DSC (red line) traces of activated $Zr_6O_4(OH)_4(bpdc\text{-}I)_6$ under a combined flow of $N_2$ (20 $cm^3$/min) and compressed air (20 $cm^3$/min).

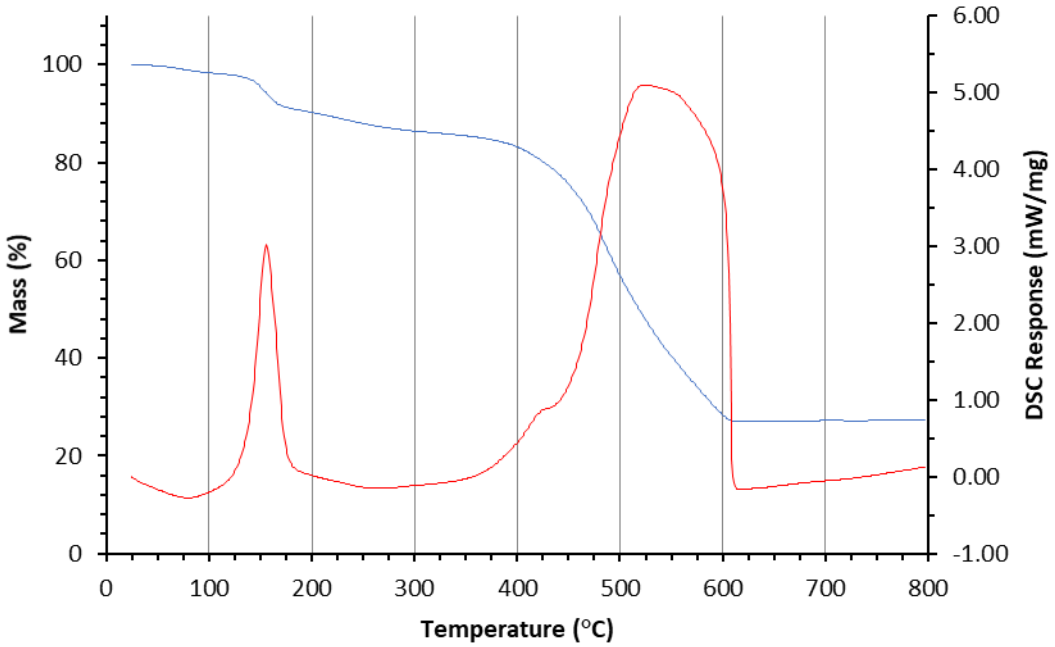


**Figure S5.9:** TG (blue line) and DSC (red line) traces of activated $Zr_6O_4(OH)_4(bpdc\text{-}IO_x)_6$ under a combined flow of $N_2$ (20 $cm^3$/min) and compressed air (20 $cm^3$/min).

**Table S5.1:** Comparison of experimental mass losses from the TG-DSC traces below 300 °C, and the calculated mass losses for $O_3H_2$ attached to each iodo group (-I=O(OH)$_2$).

| MOF | Experimental Mass Loss (%) | Calculated mass Loss (%) |
|---|---|---|
| $Zn_4O(bpdc\text{-}IO_x)_3$ | 7.88 | 6.87 |
| $Zr_6O_4(OH)_4(bpdc\text{-}IO_x)_6$ | 10.88 | 9.28 |

## 6. $^1$H NMR Spectroscopic Data

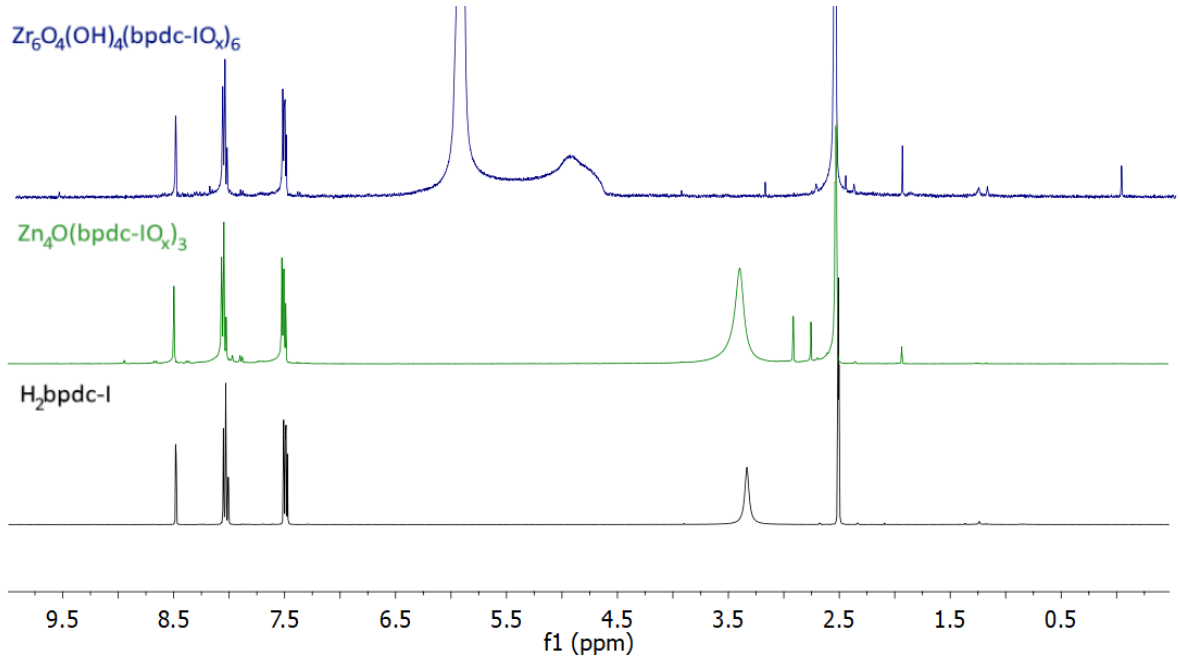


**Figure S6.1:** $^1$H NMR spectra of $H_2$bpdc-I (black trace), and digested samples of MOF after heating for 1 hour to 210 °C under $N_2$ *i.e.* this means heating above the thermal events in the MOFs. The spectrum shown in green is the digestion after heating $Zn_4O(bpdc\text{-}IO_x)_3$ and the spectrum shown in blue is the digestion after heating $Zr_6O_4(OH)_4(bpdc\text{-}IO_x)_6$. The former complex requires digestion in DCl / $d_6$-DMSO, the latter complex requires digestion in $D_2SO_4$ / $d_6$-DMSO.

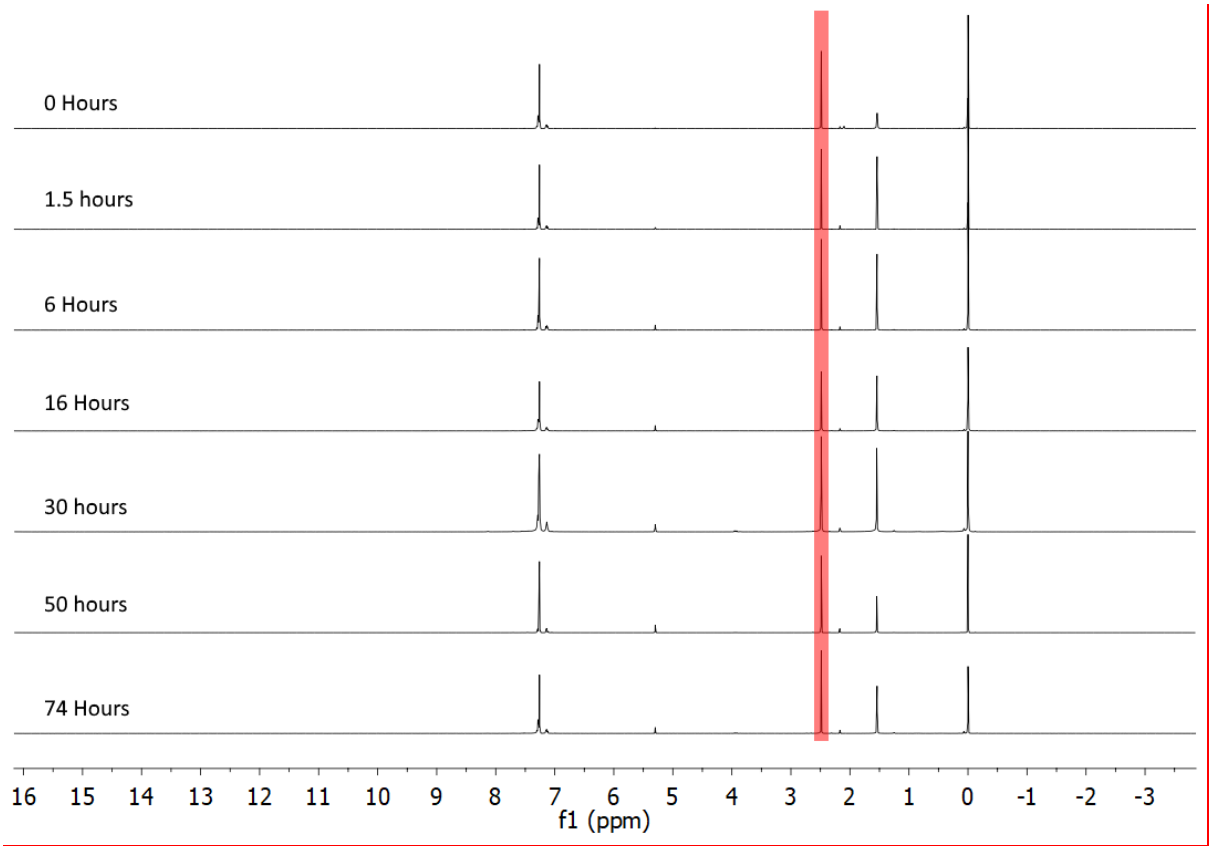


**Figure S6.2:** $^{1}H$ NMR spectra of the $CDCl_3$ solution in the reaction of Ph-$IO_2$ with thioanisole and trifluoroacetic acid after 0, 1.5, 6, 16, 30, 50 and 74 hours. Peak in red corresponds to $CH_3$ of thioanisole (2.49 ppm).[6] The peak that corresponds to $CH_3$ of (methylsulfinyl)benzene (2.73 ppm),[7] and the peak that corresponds to $CH_3$ of (methylsulfonyl)benzene (3.08 ppm),[8] are noticeably absent.

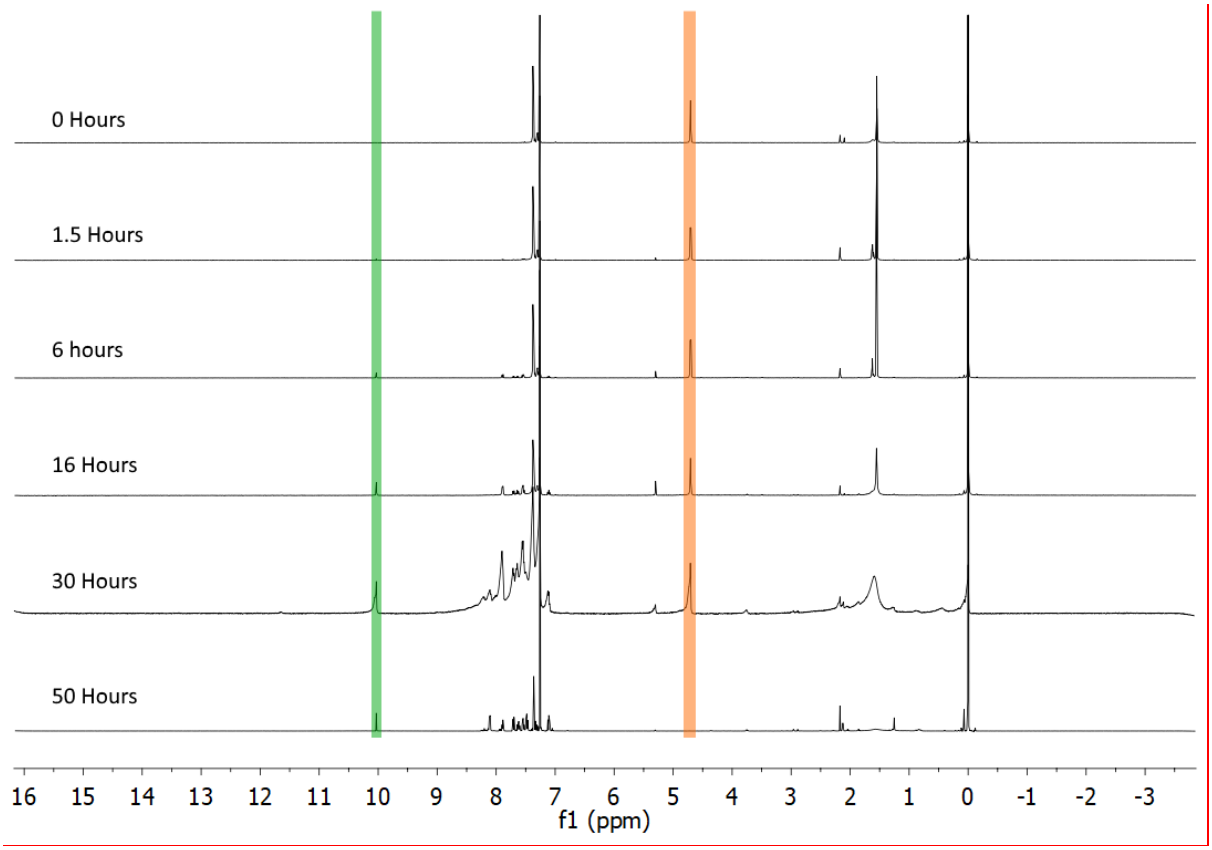


**Figure S6.3:** $^{1}H$ NMR spectra of the $CDCl_3$ solution in the reaction of Ph-$IO_2$ with benzyl alcohol and trifluoroacetic acid after 0, 1.5, 6, 16, 30 and 50 hours. Peak in orange corresponds to $CH_2$ of benzyl alcohol (4.71 ppm),[9] peak in green corresponds to CH of benzaldehyde (10.03 ppm).[10]

## 7. Mass Spectrometric Data

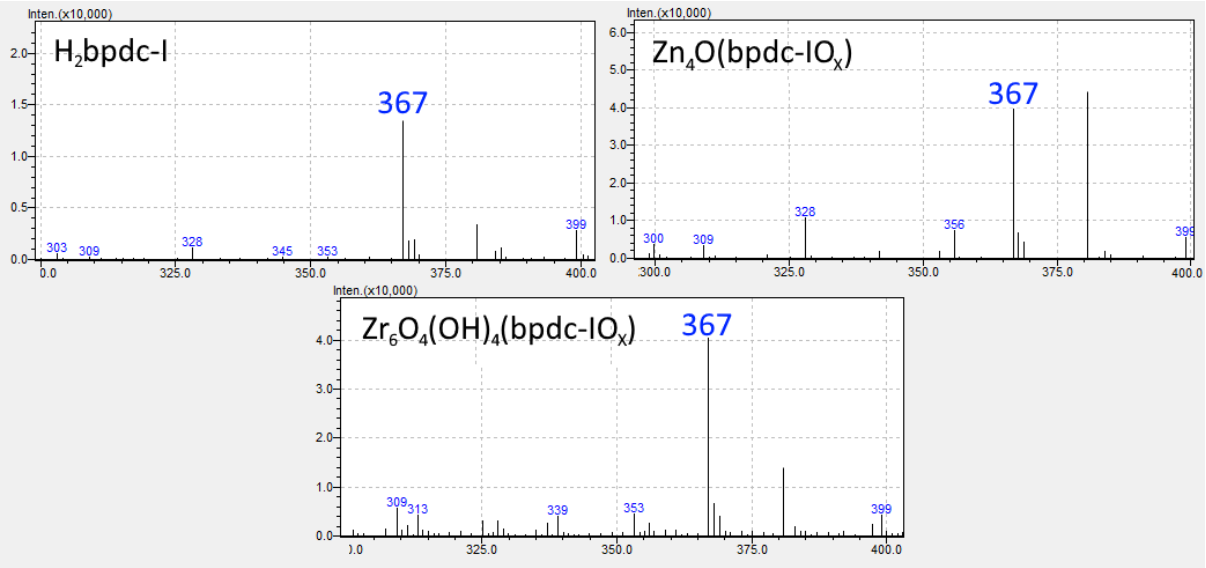


**Figure S7.1:** Low-resolution negative-mode electrospray ionisation mass spectra of $H_2$bpdc-I, and digested samples of zinc and zirconium MOFs ($Zn_4O$(bpdc-$IO_x$)$_3$ and $Zr_6O_4(OH)_4$(bpdc-$IO_x$)$_6$, respectively) recovered after heating at 210 °C under $N_2$ for 1 hour *i.e.* the ESI data were recorded after the thermolysis events. [Hbpdc-I]$^-$ = 367 *m/z*.

## 8. XPS Data

### 8.1. XPS spectra of $H_2$bpdc-I

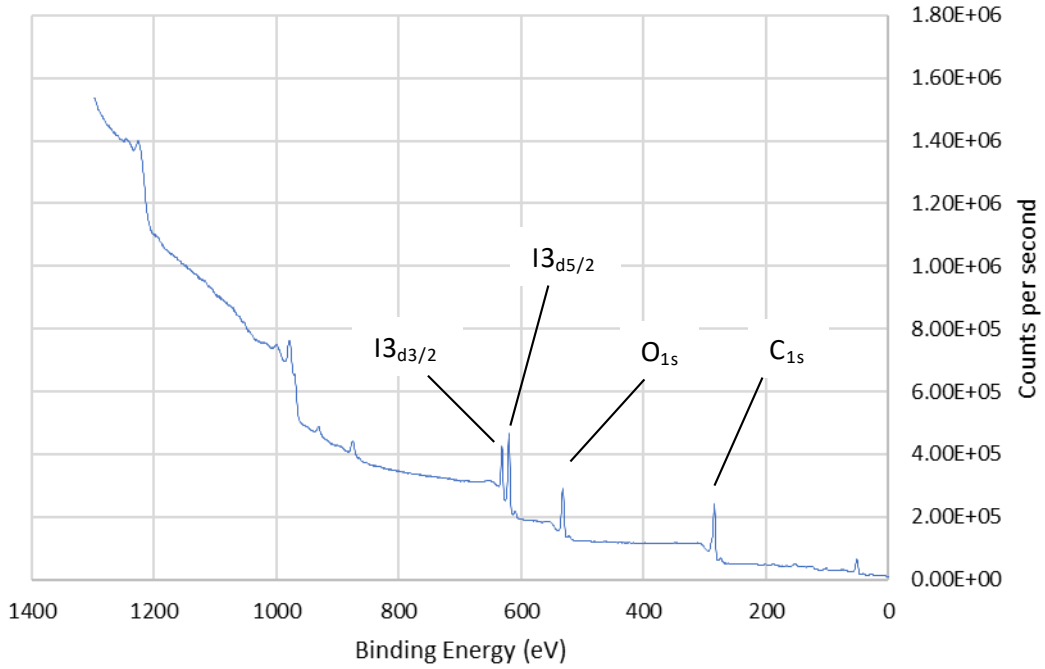


**Figure S8.1:** XPS survey spectrum of $H_2$bpdc-I, with selected peaks indicated.

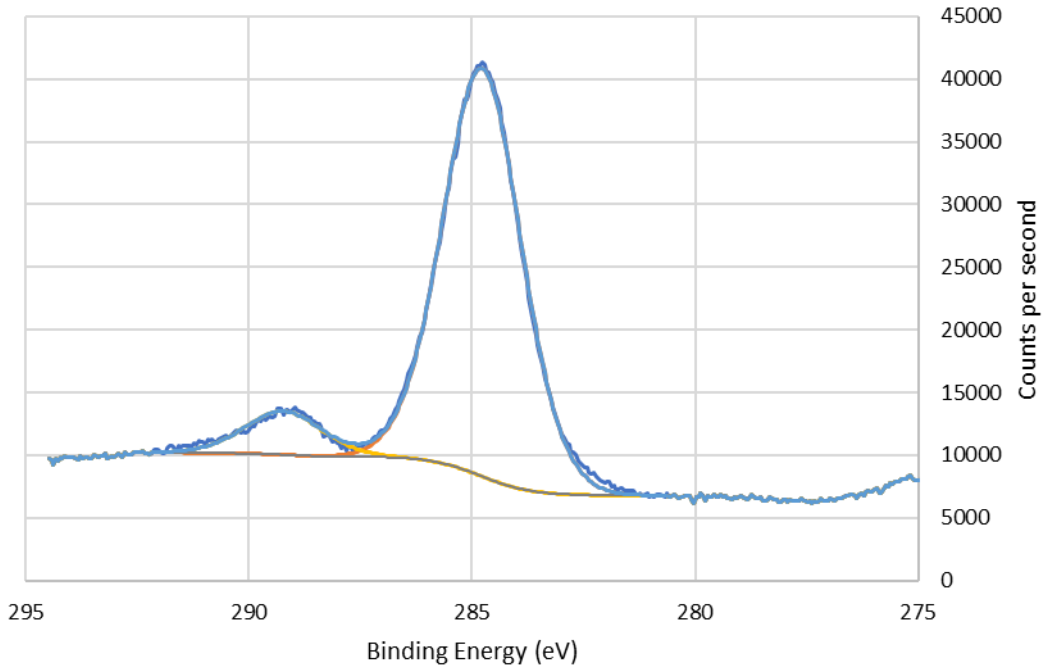


**Figure S8.2:** XPS spectrum of C $1_s$ of $H_2$bpdc-I, showing C-C peak (referenced to 284.8 eV) and O=C-O (289.2 eV). Blue line represents raw experimental response, orange line represents calculated peak corresponding to C-C, yellow line represents calculated peak corresponding to O=C-O, grey line represents background.

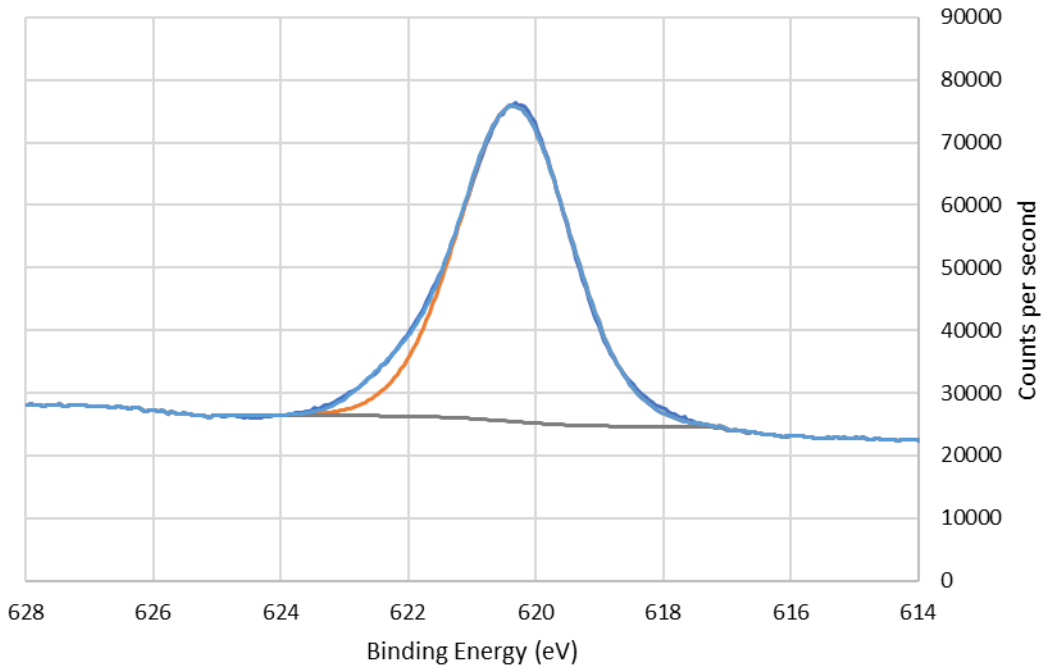


**Figure S8.3:** XPS spectrum of I $3_{d5/2}$ of $H_2$bpdc-I showing the iodine(I) peak (620.2 eV). Blue line represents raw experimental response, orange line represents calculated peak corresponding to iodine(I), grey line represents background.

## 8.2. XPS spectra of $H_2$bpdc-IO

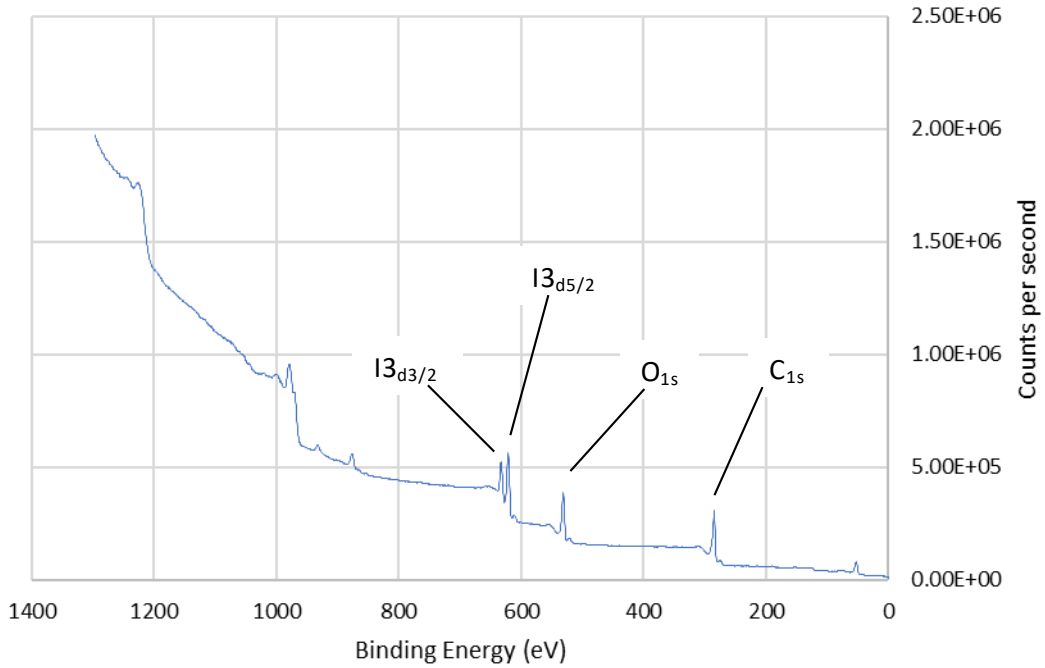


**Figure S8.4:** XPS survey spectrum of $H_2$bpdc-IO, with selected peaks indicated.

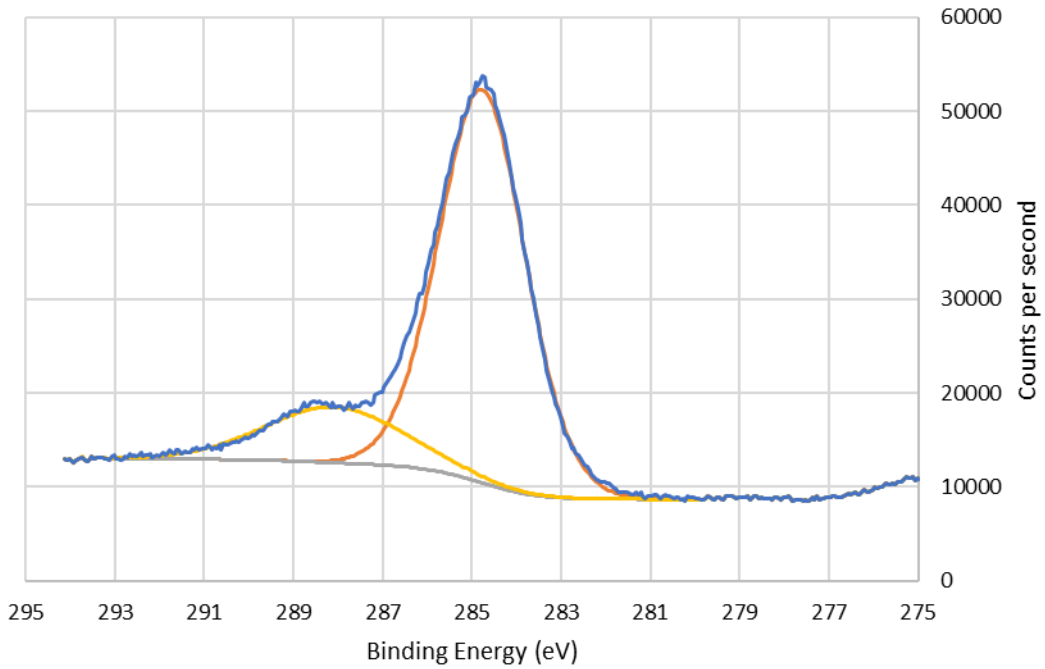


**Figure S8.5:** XPS spectrum of C $1_s$ of $H_2$bpdc-IO, showing C-C peak (referenced to 284.8 eV) and O=C-O (288.1 eV). Blue line represents raw experimental response, orange line represents calculated peak corresponding to C-C, yellow line represents calculated peak corresponding to O=C-O, grey line represents background.

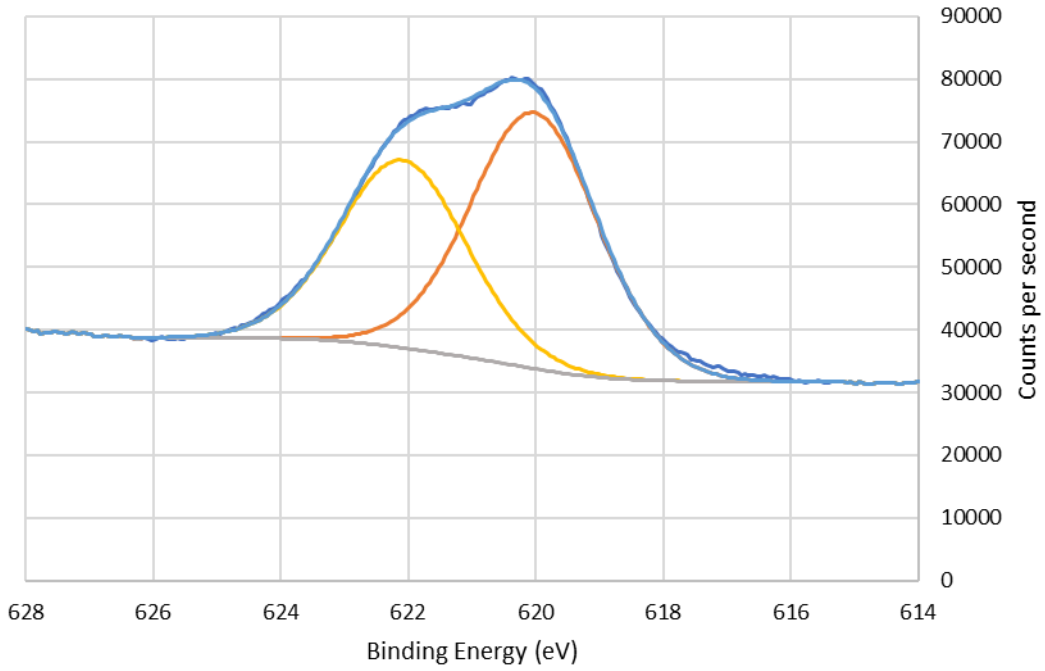


**Figure S8.6:** XPS spectrum of I $3_{d5/2}$ of $H_2$bpdc-IO showing iodine(I) peak (620.0 eV) and iodine(III) peak (622.1 eV). Blue line represents raw experimental response, orange line represents calculated peak corresponding to iodine(I), yellow line represents calculated peak corresponding to iodine(III), grey line represents background.

## 8.3. XPS spectra of Iodoxybenzene, Ph-$IO_2$

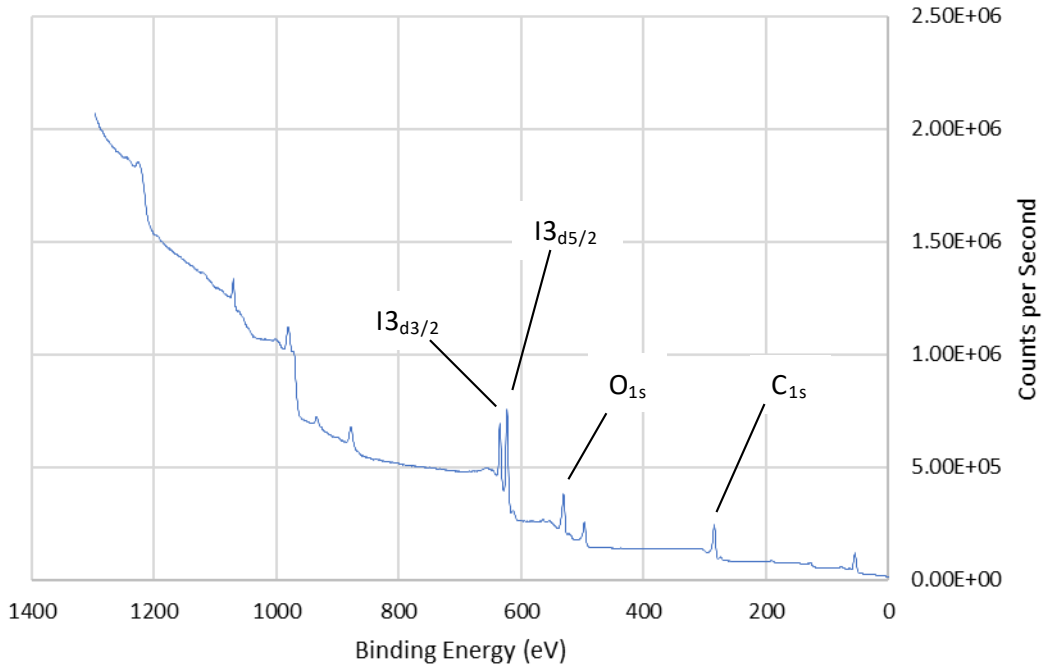


**Figure S8.7:** XPS survey spectrum of iodoxybenzene (Ph-$IO_2$), with selected peaks indicated.

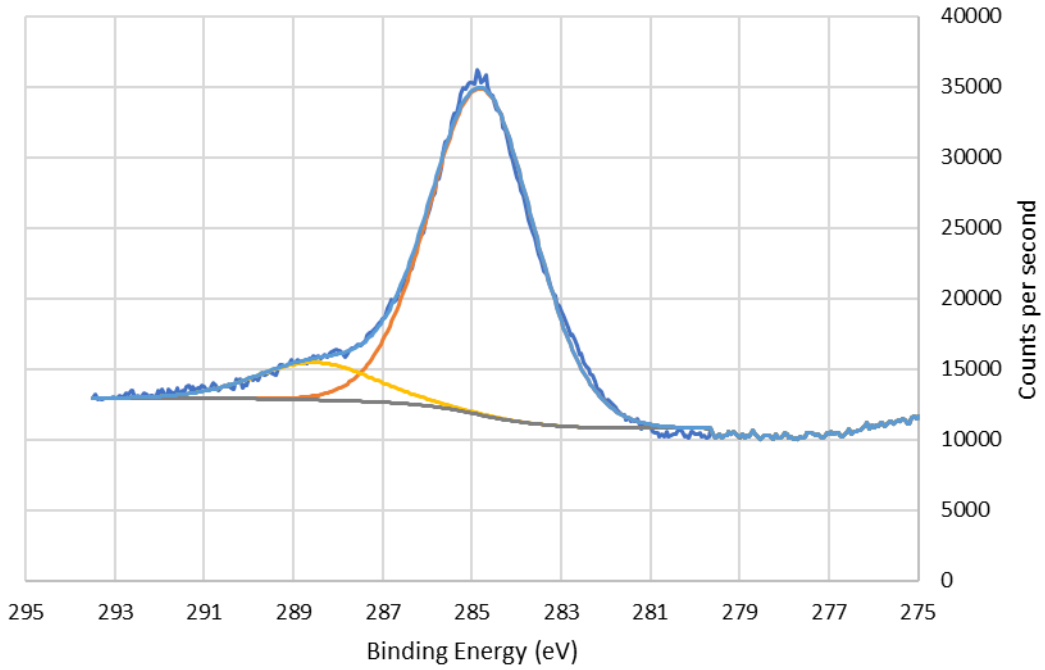


**Figure S8.8:** XPS spectrum of C $1_s$ of iodoxybenzene (Ph-$IO_2$), showing C-C peak (284.8 eV) and O=C-O (288.4 eV). Blue line represents raw experimental response, orange line represents calculated peak corresponding to C-C, yellow line represents calculated peak corresponding to O=C-O, grey line represents background.

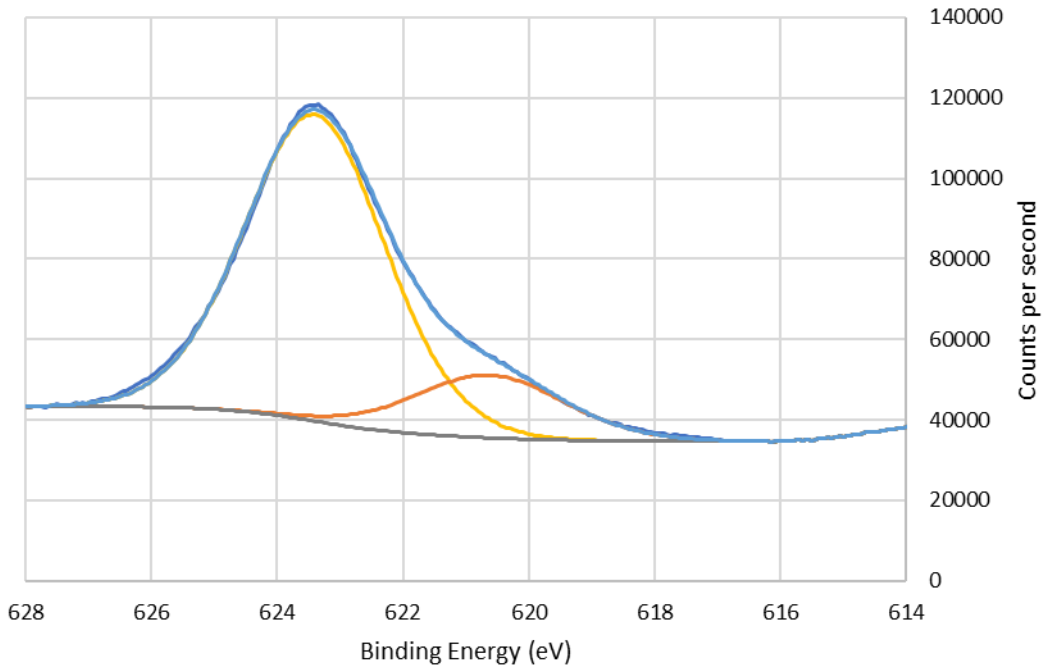


**Figure S8.9:** XPS spectrum of I $3_{d5/2}$ of iodoxybenzene (Ph-$IO_2$) showing iodine(I) peak (620.6 eV) and iodine(V) peak (623.4 eV). Blue line represents raw experimental response, orange line represents calculated peak corresponding to iodine(I), yellow line represents calculated peak corresponding to iodine(V), grey line represents background.

## 8.4. XPS spectra of $Zn_4O(bpdc\text{-}I)_3$

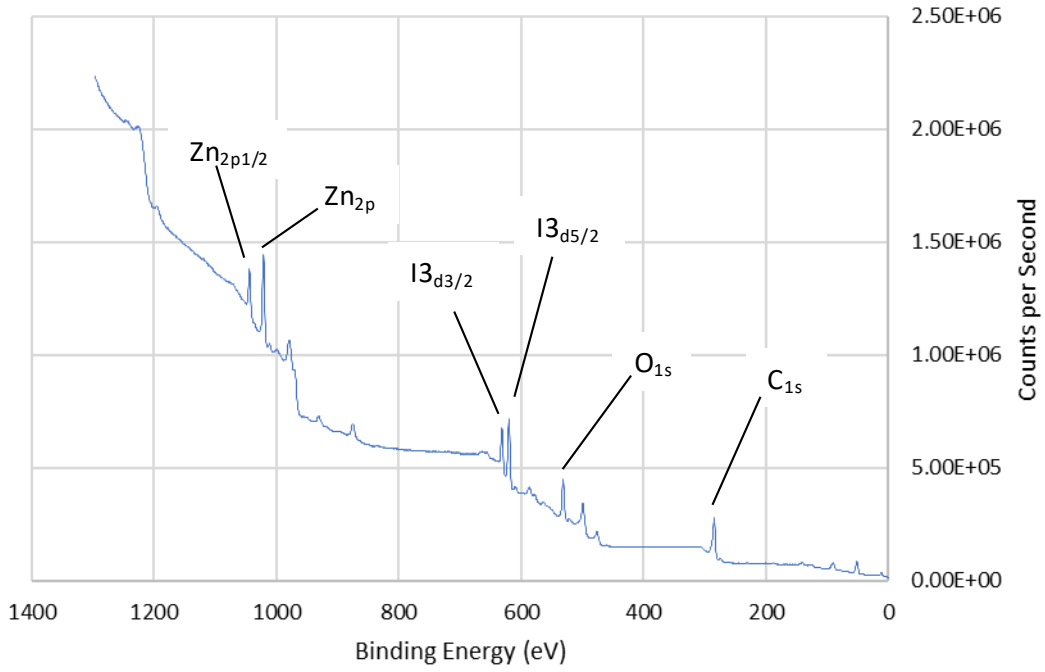


**Figure S8.10:** XPS survey spectrum of $Zn_4O(bpdc\text{-}I)_3$, with selected peaks indicated.

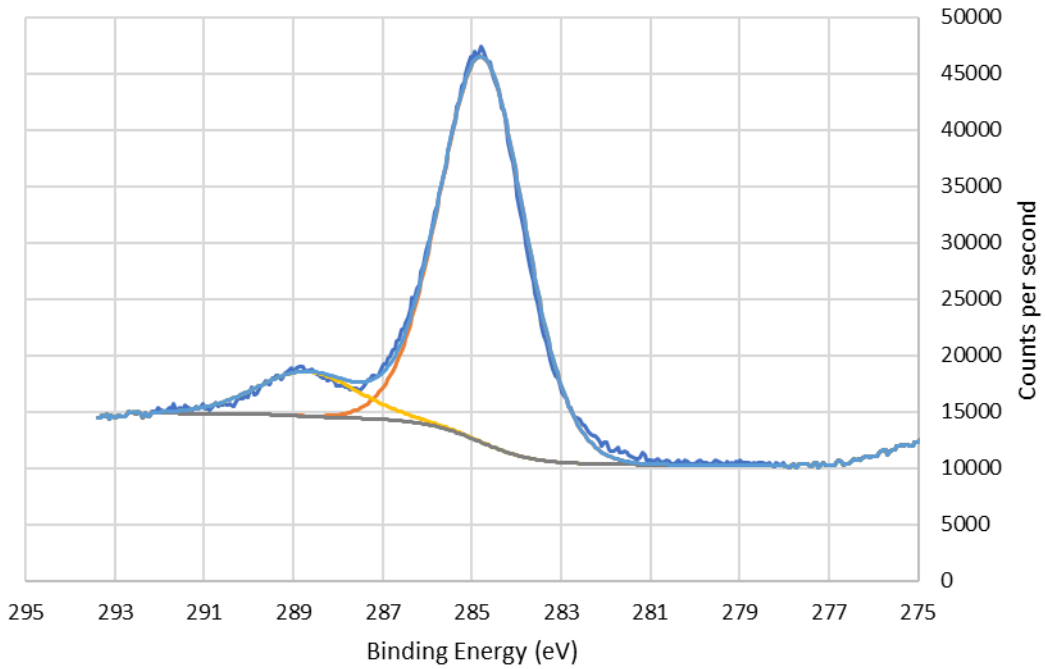


**Figure S8.11:** XPS spectrum of C $1_s$ of $Zn_4O(bpdc\text{-}I)_3$ showing C-C peak (284.8 eV) and O=C-O peak (288.7 eV). Blue line represents raw experimental response, orange line represents calculated peak corresponding to C-C, yellow line represents calculated peak corresponding to O=C-O, grey line represents background.

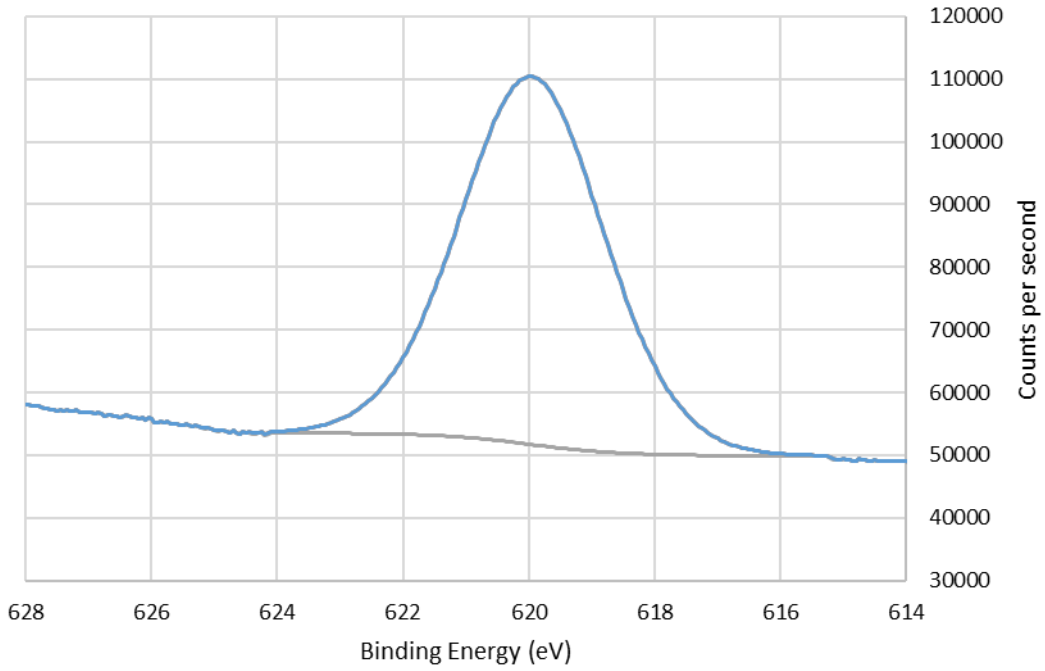


**Figure S8.12:** XPS spectrum of I $3_{d5/2}$ of $Zn_4O(bpdc\text{-}I)_3$ showing the iodine(I) peak (620.0 eV). Blue line represents raw response, grey line represents background.

## 8.5. XPS spectra of $Zn_4O(bpdc\text{-}IO_x)_3$

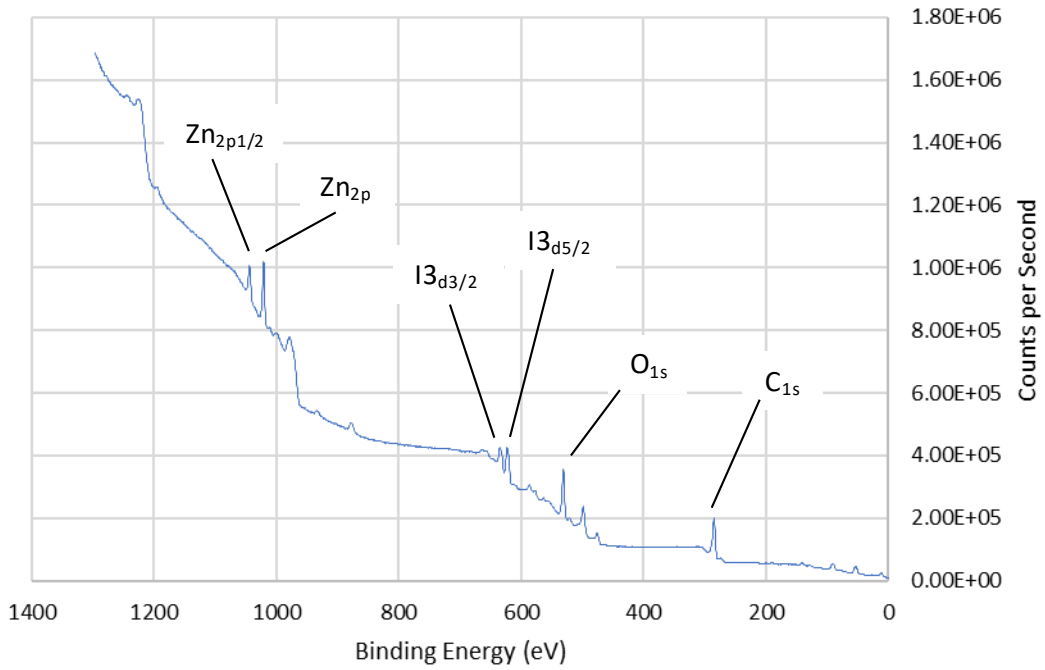


**Figure S8.13:** XPS spectrum survey of $Zn_4O(bpdc\text{-}IO_x)_3$, with selected peaks indicated.

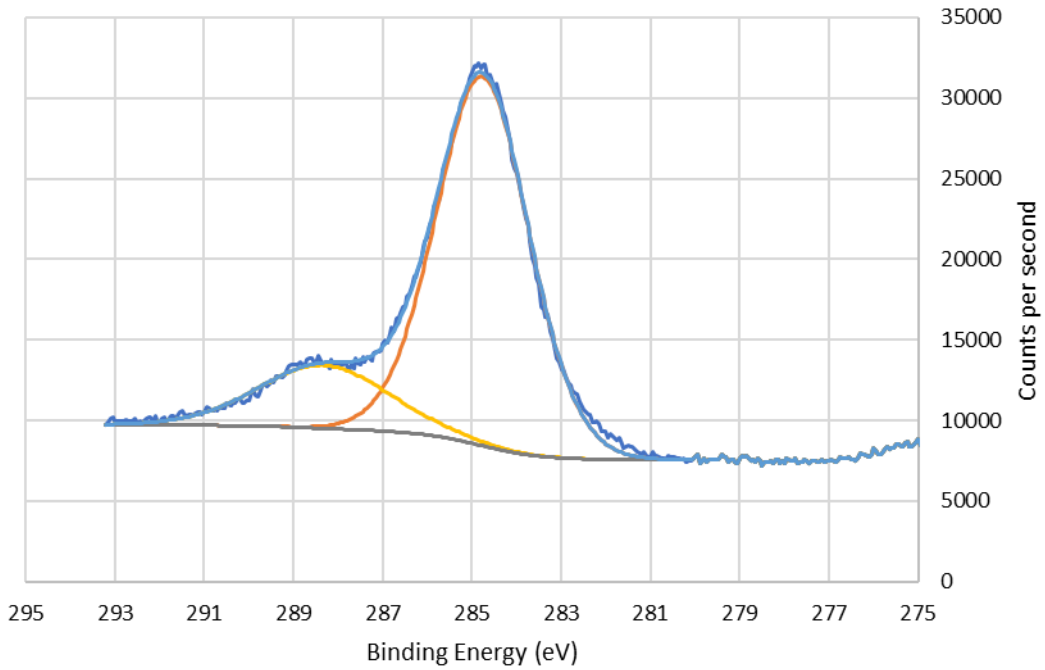


**Figure S8.14:** XPS spectrum of C $1_s$ of $Zn_4O(bpdc\text{-}IO_x)_3$ showing C-C peak (284.4 eV) and O=C-O peak (288.4 eV). Blue line represents raw response, orange line represents calculated peak corresponding to C-C, yellow line represents calculated peak corresponding to O=C-O, grey line represents background.

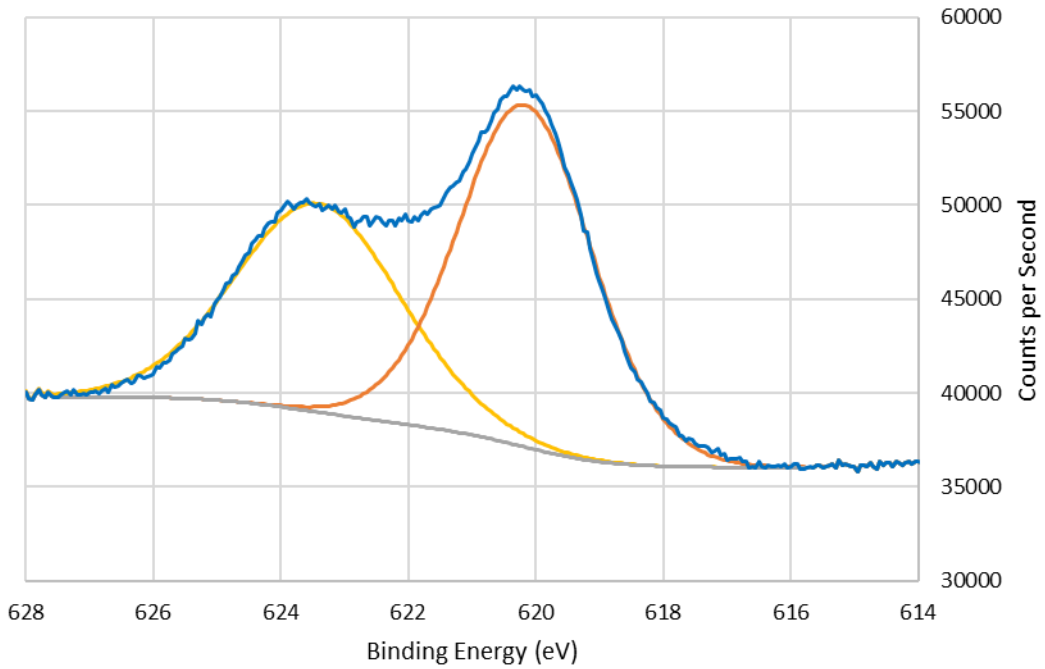


**Figure S8.15:** XPS spectrum of I $3_{d5/2}$ of $Zn_4O(bpdc\text{-}IO_x)_3$ showing iodine(I) peak (620.2 eV) and iodine(III) peak (623.7 eV). Blue line represents raw experimental response, orange line represents calculated peak corresponding to iodine(I), yellow line represents calculated peak corresponding to iodine(V), grey line represents background.

## 8.6. XPS spectra of $Zr_6O_4(OH)_4(bpdc\text{-}I)_6$

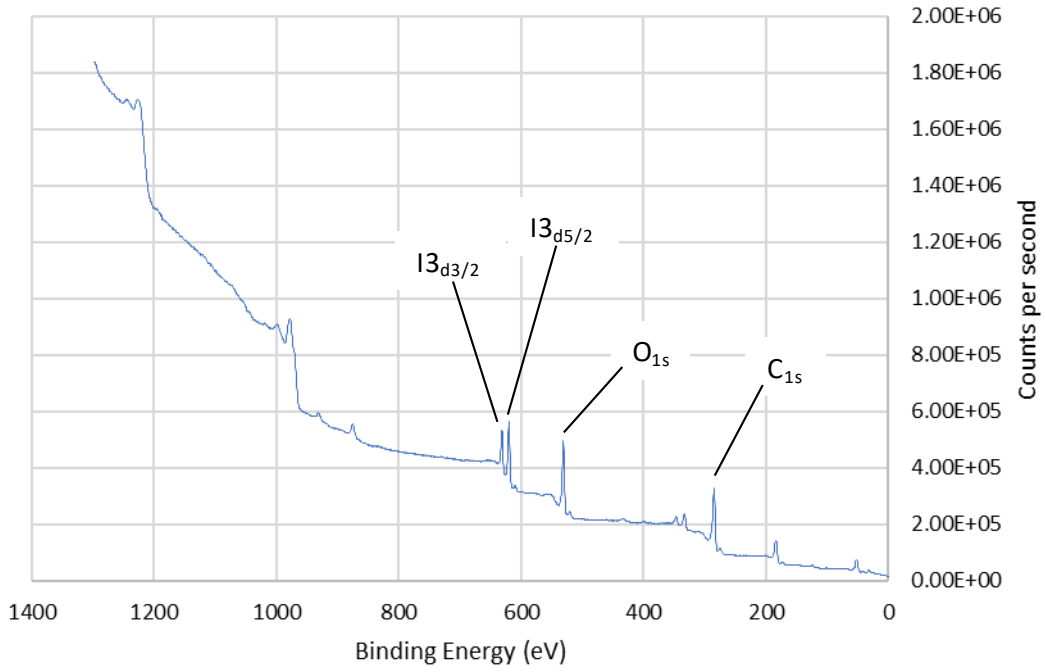


**Figure S8.16:** XPS spectrum survey of $Zr_6O_4(OH)_4(bpdc\text{-}I)_6$, with selected peaks indicated.

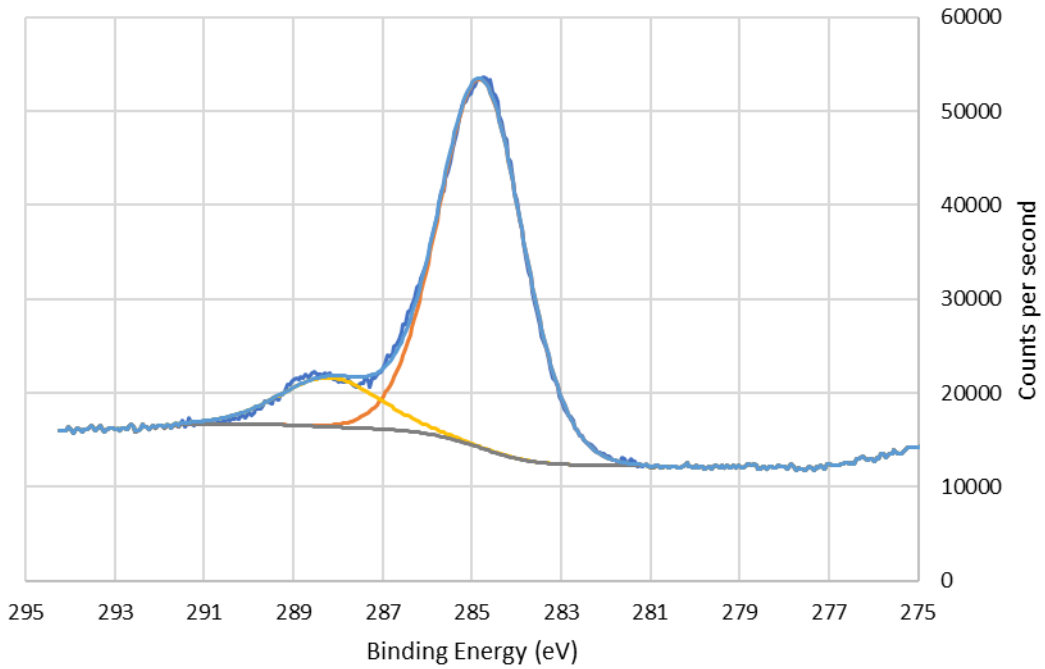


**Figure S8.17:** XPS spectrum of C $1_s$ of $Zr_6O_4(OH)_4(bpdc\text{-}I)_6$ showing C-C peak (284.8 eV) and O=C-O peak (288.2 eV). Blue line represents raw experimental response, orange line represents calculated peak corresponding to C-C, yellow line represents calculated peak corresponding to O=C-O, grey line represents background.

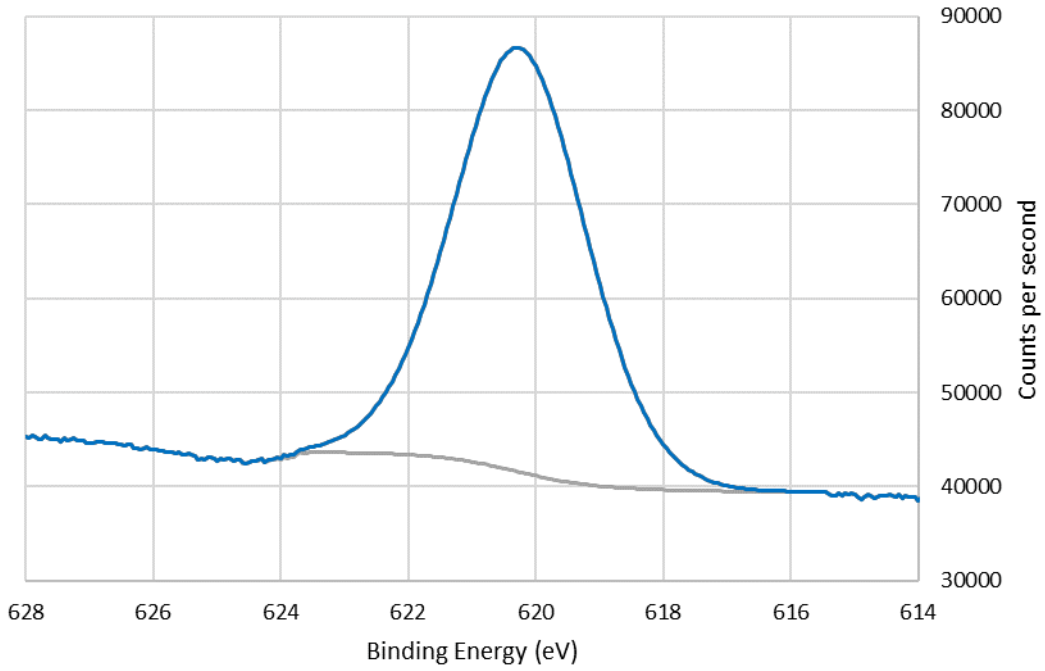


**Figure S8.18:** XPS spectrum of $I3_{d5/2}$ of $Zr_6O_4(OH)_4(bpdc\text{-}I)_6$ showing iodine(I) peak (620.2 eV). Blue line represents raw experimental response, orange line represents calculated peak corresponding to iodine(I), grey line represents background.

## 8.7. XPS spectra of $Zr_6O_4(OH)_4(bpdc\text{-}IO_x)_6$

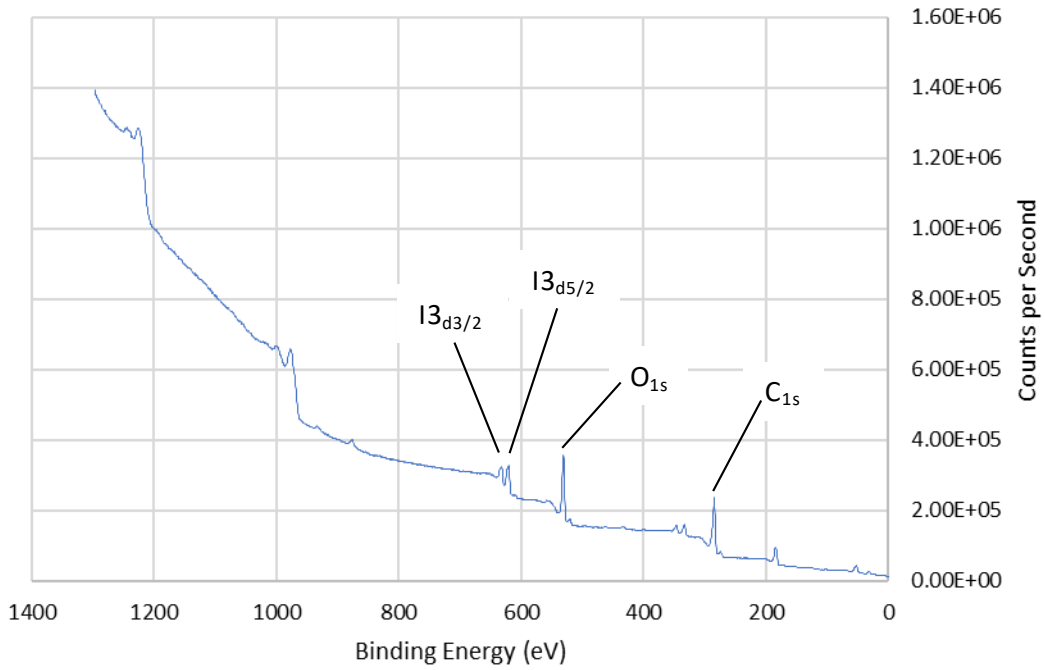


**Figure S8.19:** XPS spectrum survey of $Zr_6O_4(OH)_4(bpdc\text{-}IO_x)_6$, with selected peaks indicated.

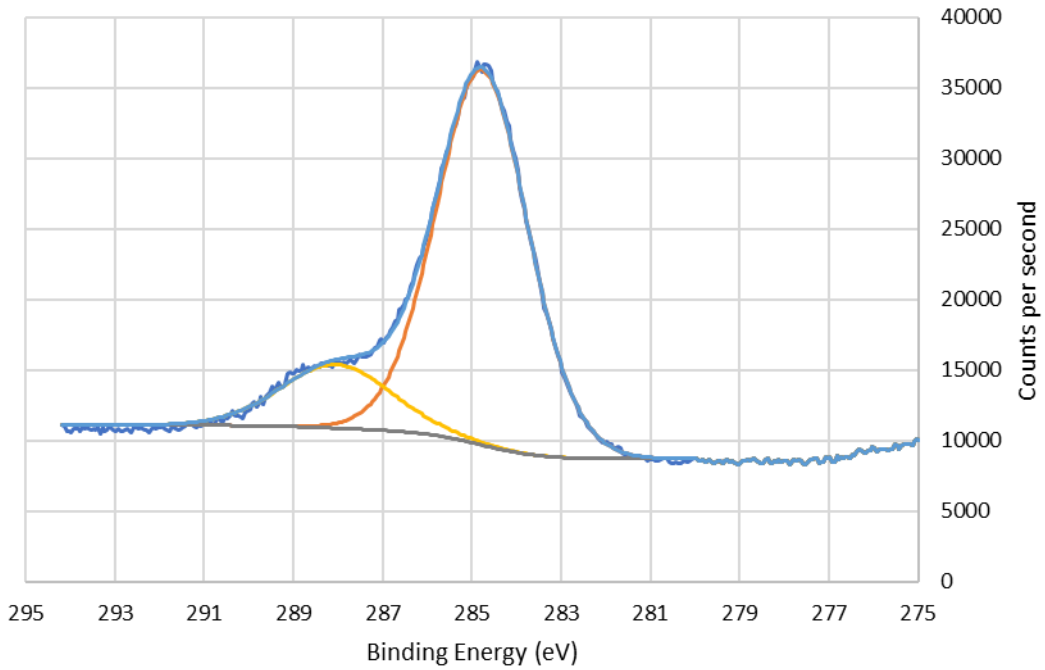


**Figure S8.20:** XPS spectrum of C $1_s$ of $Zr_6O_4(OH)_4(bpdc\text{-}IO_x)_6$ showing C-C peak (284.8 eV) and O=C-O peak (288.0 eV). Blue line represents raw experimental response, orange line represents calculated peak corresponding to C-C, yellow line represents calculated peak corresponding to O=C-O, grey line represents background.

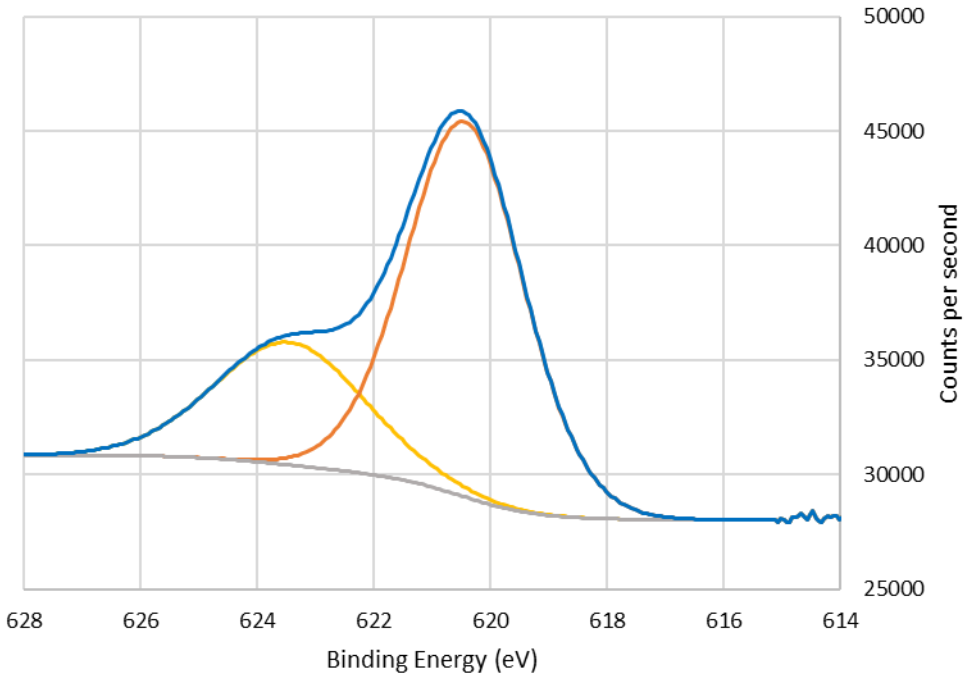


**Figure S8.21:** XPS spectrum of I $3_{d5/2}$ of $Zr_6O_4(OH)_4(bpdc\text{-}IO_x)_6$ showing iodine(I) peak (620.1 eV) and iodine(V) peak (623.0 eV). Blue line represents raw experimental response, orange line represents calculated peak corresponding to iodine(I), yellow line represents calculated peak corresponding to iodine(V), grey line represents background.

## 8.8. XPS spectra of $Zr_6O_4(OH)_4(bpdc\text{-}IO_x)_6$ Post-Thermolysis

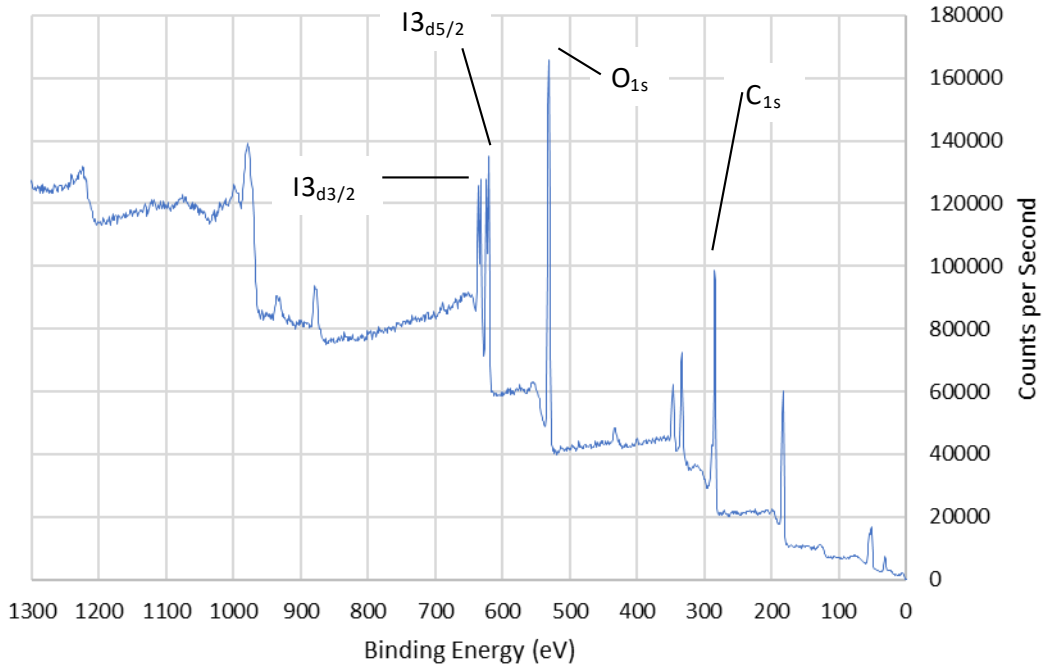


**Figure S8.22:** XPS spectrum survey of $Zr_6O_4(OH)_4(bpdc\text{-}IO_x)_6$ post-thermolysis, with selected peaks indicated.

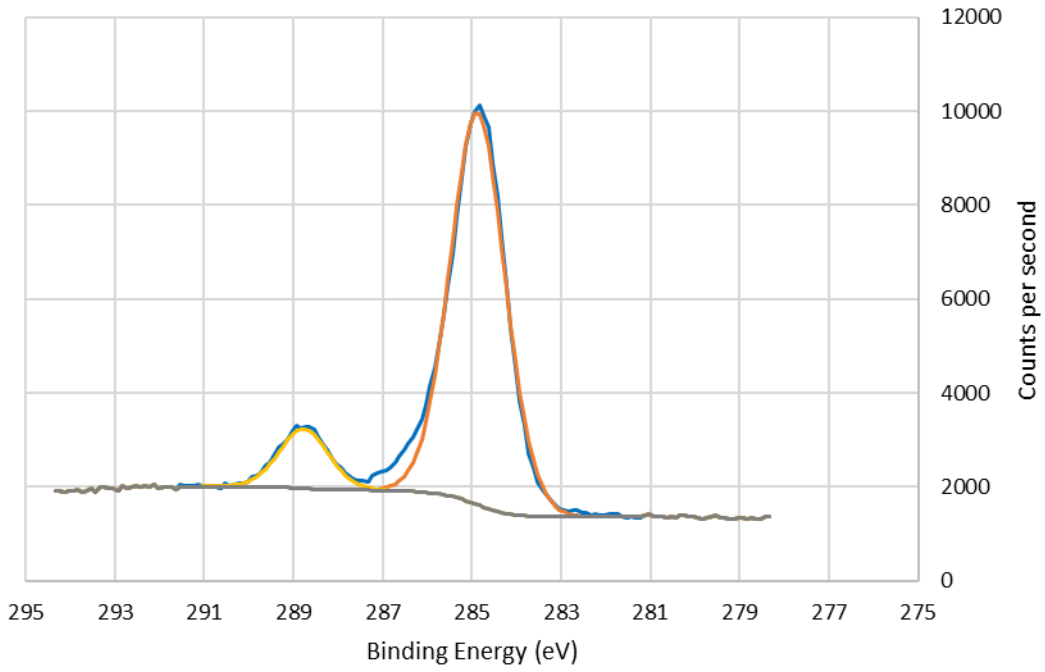


**Figure S8.23:** XPS spectrum of C $1_s$ of $Zr_6O_4(OH)_4(bpdc\text{-}IO_x)_6$ post-thermolysis showing C-C peak (284.8 eV) and O=C-O peak (288.0 eV). Blue line represents raw experimental response, orange line represents calculated peak corresponding to C-C, yellow line represents calculated peak corresponding to O=C-O, grey line represents background.

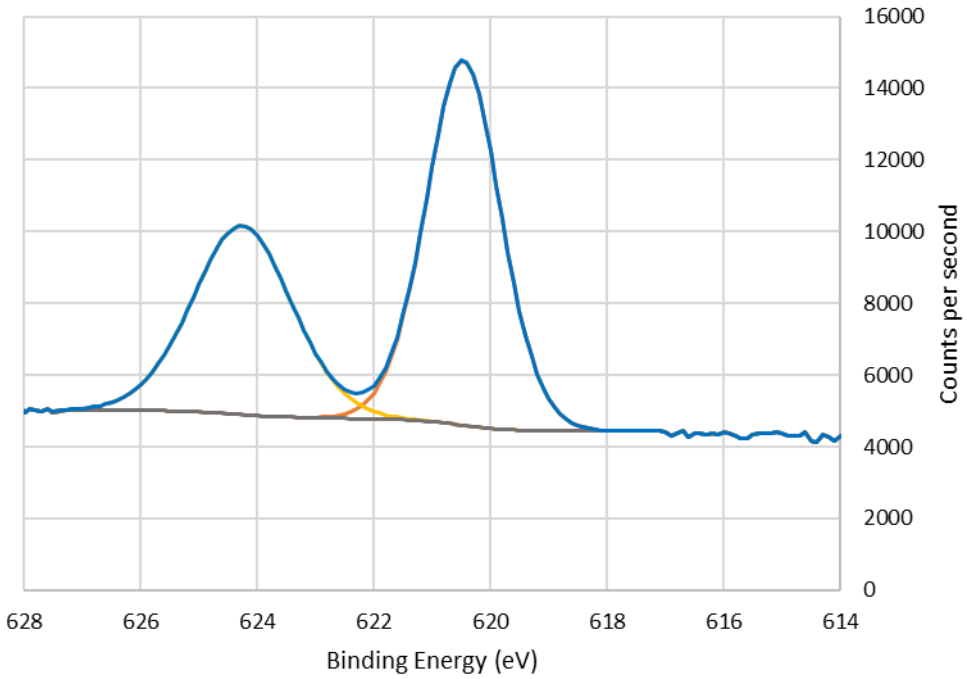


**Figure S8.24:** XPS spectrum of I $3_{d5/2}$ of $Zr_6O_4(OH)_4(bpdc\text{-}IO_x)_6$ post-thermolysis showing iodine(I) peak (620.4 eV) and iodine(V) peak (624.1 eV). Blue line represents raw experimental response, orange line represents calculated peak corresponding to iodine(I), yellow line represents calculated peak corresponding to iodine(V), grey line represents background.

## 9. $N_2$ Gas Sorption at 77 K

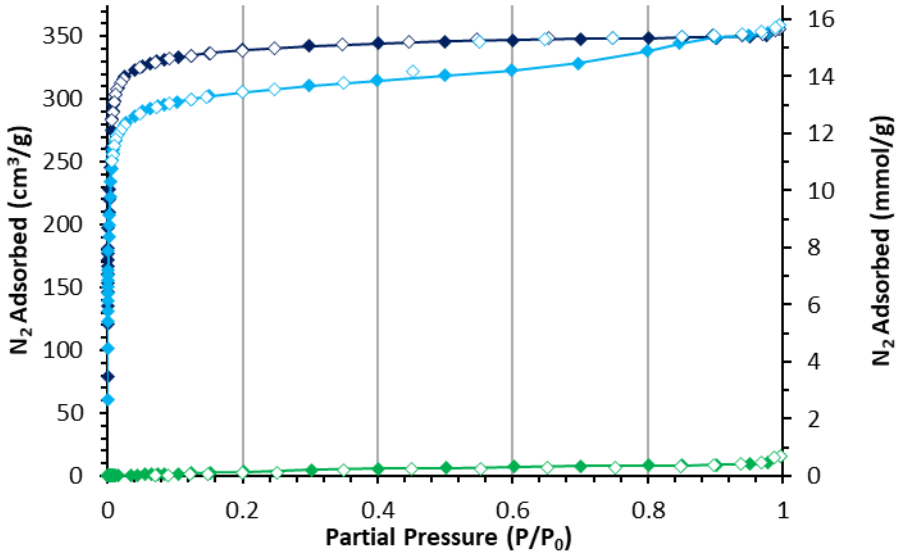


**Figure S9.1:** $N_2$ sorption isotherms of $Zn_4O(bpdc\text{-}I)_3$ (dark blue), $Zn_4O(bpdc\text{-}IO_x)_3$ (light blue) and $Zn_4O(bpdc\text{-}IO_x)_3$ after thermolysis (green). Closed symbols represent adsorption, open symbols represent desorption.

BET Tables for Zinc MOFs from $N_2$ adsorption at 77 K.

| BET summary for $Zn_4O(bpdc\text{-}I)_3$ | | |
|---|---|---|
| Slope | 2.528 | |
| Intercept | 1.765e-03 | |
| Correlation coefficient, r | 0.999976 | |
| C constant | 1433.462 | |
| Surface Area | 1376.414 | |
| Relative Pressure | Volume @ STP | 1 / [W((Po/P) - 1)] |
| 8.01449e-03 | 290.2299 | 2.2273e-02 |
| 9.03781e-03 | 295.0936 | 2.4728e-02 |
| 1.00921e-02 | 298.8305 | 2.7297e-02 |
| 1.19917e-02 | 303.5481 | 3.1992e-02 |
| 1.52389e-02 | 308.8887 | 4.0084e-02 |
| 2.61900e-02 | 317.8581 | 6.7698e-02 |
| 4.00628e-02 | 323.3369 | 1.0327e-01 |

| BET summary for $Zn_4O(bpdc\text{-}IO_x)_3$ | | |
|---|---|---|
| Slope | 2.851 | |
| Intercept | 2.230e-03 | |
| Correlation coefficient, r | 0.999993 | |
| C constant | 1279.495 | |
| Surface Area | 1220.668 | |
| Relative Pressure | Volume @ STP | 1 / [W((Po/P) - 1)] |
| 8.05460e-03 | 256.3673 | 2.5342e-02 |
| 9.11816e-03 | 260.2868 | 2.8287e-02 |
| 1.00408e-02 | 262.9024 | 3.0868e-02 |
| 1.21162e-02 | 267.2554 | 3.6718e-02 |
| 1.51245e-02 | 271.7263 | 4.5219e-02 |
| 2.74980e-02 | 281.3195 | 8.0419e-02 |
| 4.09215e-02 | 286.7966 | 1.1903e-01 |

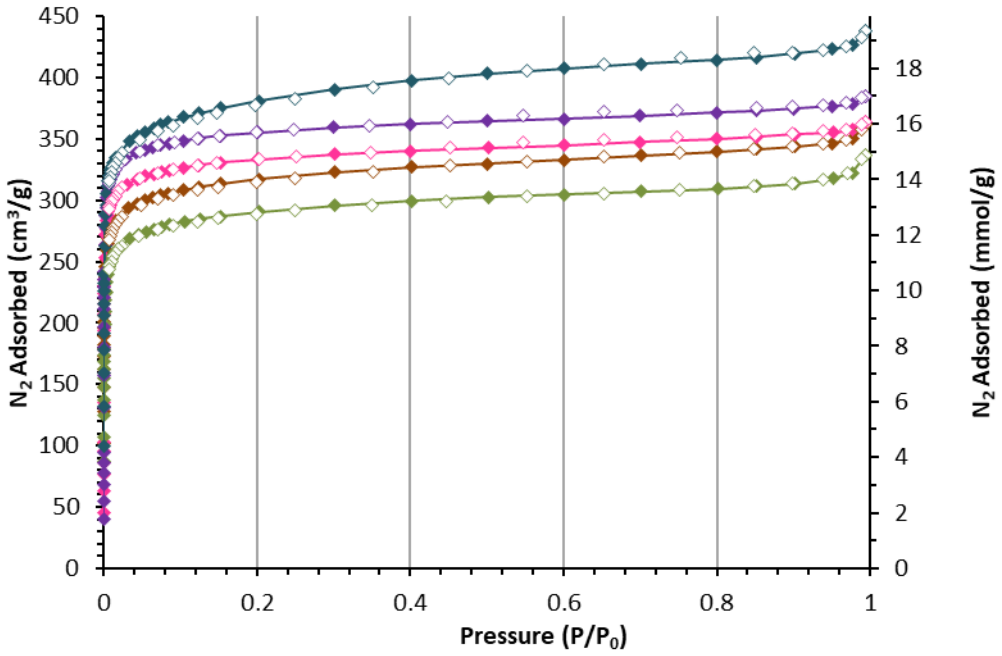


**Figure S9.2**: $N_2$ sorption isotherms of $Zr_6O_4(OH)_4(bpdc\text{-}I)_6$ (purple), $Zr_6O_4(OH)_4(bpdc\text{-}IO_x)_6$ (magenta); and $Zr_6O_4(OH)_4(bpdc\text{-}IO_x)_6$ after thermolysis (dark green), $Zr_6O_4(OH)_4(bpdc\text{-}IO_x)_6$ after oxidation of benzyl alcohol (brown), $Zr_6O_4(OH)_4(bpdc\text{-}IO_x)_6$ after oxidation of thioanisole (light green). Closed symbols represent adsorption, open symbols represent desorption.

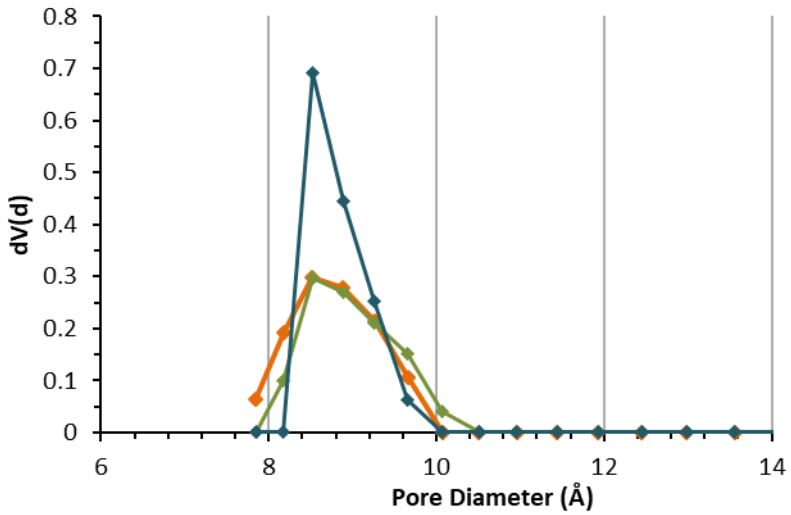


**Figure S9.3:** Pore diameter distributions of $Zr_6O_4(OH)_4(bpdc\text{-}IO_x)_6$ after thermolysis (dark green) and after reaction with benzyl alcohol (brown) and thioanisole (green). Pore diameters derived from QSDFT equilibrium model kernel with slit/cylindrical pores.

**Table S9.1:** Accessible BET surface areas and pore volumes of $Zr_6O_4(OH)_4(bpdc\text{-}I)_6$, $Zr_6O_4(OH)_4(bpdc\text{-}IO_x)_6$, and $Zr_6O_4(OH)_4(bpdc\text{-}IO_x)_6$ after thermolysis and reactions with benzyl alcohol and thioanisole from $N_2$ gas adsorption measurements at 77 K.

| MOF | BET Surface Area ($m^2/g$) | Pore Volume ($cm^3/g$) |
|---|---|---|
| $Zr_6O_4(OH)_4(bpdc\text{-}I)_6$ | 1423 | 0.55 |
| $Zr_6O_4(OH)_4(bpdc\text{-}IO_x)_6$ | 1335 | 0.52 |
| $Zr_6O_4(OH)_4(bpdc\text{-}IO_x)_6 \rightarrow Zr_6O_4(OH)_4(bpdc\text{-}I)_6$ ***i.e.*** **Post heating to 210 °C for 1 hour** | 1484 | 0.59 |
| $Zr_6O_4(OH)_4(bpdc\text{-}IO_x)_6 \rightarrow Zr_6O_4(OH)_4(bpdc\text{-}I)_6$ ***i.e.*** **Post reaction with thioanisole** | 1144 | 0.45 |
| $Zr_6O_4(OH)_4(bpdc\text{-}IO_x)_6 \rightarrow Zr_6O_4(OH)_4(bpdc\text{-}I)_6$ ***i.e.*** **Post reaction with benzyl alcohol** | 1251 | 0.49 |

| BET summary for $Zr_6O_4(OH)_4(bpdc\text{-}I)_6$ | | |
|---|---|---|
| Slope | 2.447 | |
| Intercept | 8.001e-04 | |
| Correlation | 0.999996 | |
| C constant | 3059.422 | |
| Surface Area | 1422.674 | |
| Relative Pressure | Volume @ | 1 / [W((Po/P) - |
| 8.10410e-03 | 316.6463 | 2.0645e-02 |
| 9.06373e-03 | 318.5324 | 2.2975e-02 |
| 1.00617e-02 | 320.2085 | 2.5397e-02 |
| 1.21245e-02 | 321.3607 | 3.0558e-02 |
| 1.51515e-02 | 324.9145 | 3.7885e-02 |
| 2.91027e-02 | 333.8645 | 7.1837e-02 |
| 4.23456e-02 | 338.4838 | 1.0452e-01 |

| BET summary for $Zr_6O_4(OH)_4(bpdc\text{-}IO_X)_6$ | | |
|---|---|---|
| Slope | 2.606 | |
| Intercept | 9.571e-04 | |
| Correlation | 0.999997 | |
| C constant | 2724.238 | |
| Surface Area | 1335.627 | |
| Relative Pressure | Volume @ | 1 / [W((Po/P) - |
| 7.09460e-03 | 294.1801 | 1.9434e-02 |
| 8.02759e-03 | 296.2355 | 2.1858e-02 |
| 9.05526e-03 | 298.1482 | 2.4523e-02 |
| 1.00549e-02 | 299.7367 | 2.7113e-02 |
| 1.20698e-02 | 300.6045 | 3.2519e-02 |
| 1.49927e-02 | 303.7922 | 4.0089e-02 |
| 3.06928e-02 | 313.0618 | 8.0929e-02 |

| BET summary for $Zr_6O_4(OH)_4(bpdc\text{-}IO_X)_6$ after heating to 210 °C | | |
|---|---|---|
| Slope | 2.345 | |
| Intercept | 1.244e-03 | |
| Correlation coefficient, r | 0.999999 | |
| C constant | 1885.741 | |
| Surface Area | 1484.302 | |
| Relative Pressure | Volume @ STP | 1 / [W((Po/P) - 1)] |
| 8.01227e-03 | 322.6822 | 2.0028e-02 |
| 9.00749e-03 | 325.1330 | 2.2368e-02 |
| 9.98093e-03 | 327.2129 | 2.4652e-02 |
| 1.20631e-02 | 330.5669 | 2.9555e-02 |
| 1.50712e-02 | 334.4571 | 3.6606e-02 |
| 3.34983e-02 | 348.0108 | 7.9686e-02 |
| 4.45260e-02 | 352.6563 | 1.0573e-01 |

| BET summary for $Zr_6O_4(OH)_4(bpdc\text{-}IO_X)_6$ after reaction with benzyl alcohol | | |
|---|---|---|
| **Slope** | 2.783 | |
| **Intercept** | 1.289e-03 | |
| **Correlation coefficient, r** | 0.999998 | |
| **C constant** | 2160.147 | |
| **Surface Area** | 1250.919 | |
| **Relative Pressure** | **Volume @** | **1 / [W((Po/P) -** |
| 8.06543e-03 | 274.0436 | 2.3740e-02 |
| 9.07829e-03 | 276.0728 | 2.6552e-02 |
| 1.00237e-02 | 277.6829 | 2.9175e-02 |
| 1.20451e-02 | 279.8937 | 3.4853e-02 |
| 1.50136e-02 | 283.1332 | 4.3075e-02 |
| 3.26952e-02 | 293.5820 | 9.2119e-02 |
| 4.41789e-02 | 297.4688 | 1.2432e-01 |

| BET summary for $Zr_6O_4(OH)_4(bpdc\text{-}IO_X)_6$ after reaction with thioanisole | | |
|---|---|---|
| **Slope** | 3.041 | |
| **Intercept** | 1.570e-03 | |
| **Correlation coefficient,** | 0.999996 | |
| **C constant** | 1938.423 | |
| **Surface Area** | 1144.493 | |
| **Relative Pressure** | **Volume @** | **1 / [W((Po/P) -** |
| 8.06589e-03 | 248.6528 | 2.6166e-02 |
| 9.08645e-03 | 250.6567 | 2.9271e-02 |
| 1.00111e-02 | 252.2099 | 3.2081e-02 |
| 1.21074e-02 | 255.7715 | 3.8339e-02 |
| 1.49815e-02 | 258.7187 | 4.7037e-02 |
| 3.33866e-02 | 268.5650 | 1.0290e-01 |
| 4.49873e-02 | 272.0372 | 1.3855e-01 |

## 10. Gas Chromatography – Mass Spectrometry

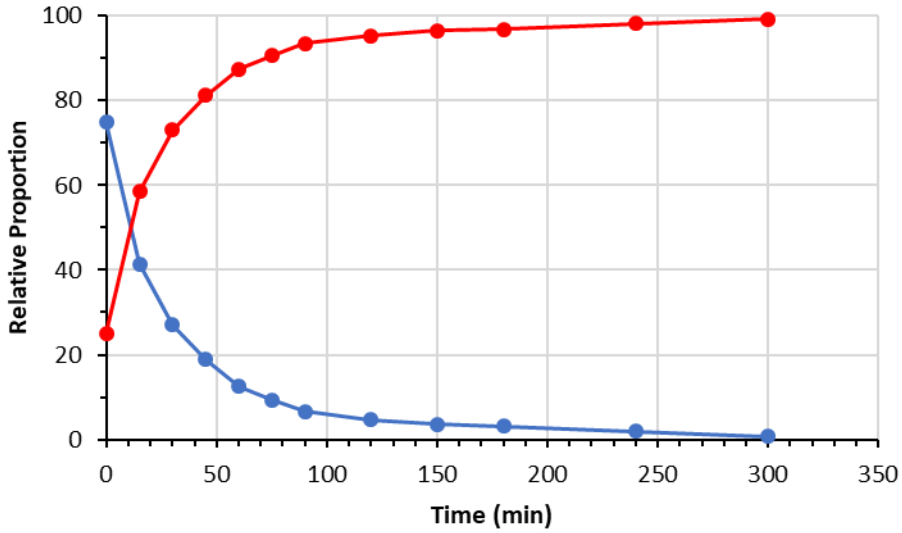


**Figure S10.1:** Relative proportions of benzyl alcohol (blue) and benzaldehyde (red) according to GC-MS analysis.

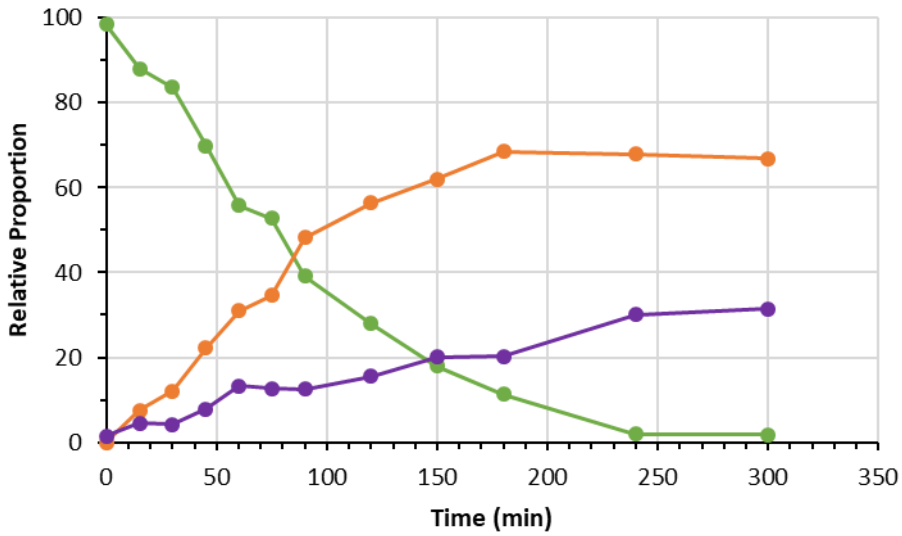


**Figure S10.2:** Relative proportions of thioanisole (green), (methylsulfinyl)benzene (orange) and (methylsulfonyl)benzene (purple) according to GC-MS analysis.

## 11. References


1 D. F. Taber, R. A. Hassan, P. W. DeMatteo, *Organic Syntheses* **2013**, *90*, 350-357.

2 W. E. Dasent, T. C. Waddington, *Journal of the Chemical Society (Resumed)* **1960**, 2429-2432.

3 R. Babarao, C. J. Coghlan, D. Rankine, W. M. Bloch, G. K. Gransbury, H. Sato, S. Kitagawa, C. J. Sumby, M. R. Hill, C. J. Doonan, *Chemical Communications* **2014**, *50*, 3238-3241.

4 R. J. Marshall, C. L. Hobday, C. F. Murphie, S. L. Griffin, C. A. Morrison, S. A. Moggach, R. S. Forgan, *Journal of Materials Chemistry A* **2016**, *4*, 6955-6963.

5 M. S. Yusubov, A. A. Zagulyaeva, V. V. Zhdankin, *Chemistry – A European Journal* **2009**, *15*, 11091-11094.

6 S. Perumal, R. Chandrasekaran, S. Selvaraj, M. Ganesan, D. A. Wilson, *Magnetic Resonance in Chemistry* **2000**, *38*, 55-57.

7 Y. Yuan, X. Shi, W. Liu, *Synlett* **2011**, *2011*, 559-564.

8 Abraham, R. J.; Byrne, J. J.; Griffiths, L., *Magnetic Resonance in Chemistry*, **2008**, *46*, 667-675.

9 R. Cano, M. Yus, D. J. Ramón, *Tetrahedron* **2011**, *67*, 8079-8085.

10 N. Jiang, A. J. Ragauskas, *Organic Letters* **2005**, *7*, 3689-3692.